

Complementary views on electron spectra: From Fluctuation Diagnostics to real space correlations

O. Gunnarsson,¹ J. Merino,² T. Schäfer,^{3,4,5} G. Sangiovanni,⁶ G. Rohringer,⁷ and A. Toschi³

¹ *Max-Planck-Institut für Festkörperforschung, Heisenbergstrasse 1, D-70569 Stuttgart, Germany*

² *Departamento de Física Teórica de la Materia Condensada,*

*Condensed Matter Physics Center (IFIMAC) and Instituto Nicolás Cabrera,
Universidad Autónoma de Madrid, Madrid 28049, Spain*

³ *Institute of solid state physics, Vienna University of Technology, 1040 Vienna, Austria*

⁴ *Centre de Physique Théorique, École Polytechnique,
CNRS, Université Paris-Saclay, 91128 Palaiseau, France*

⁵ *Collège de France, 11 place Marcelin Berthelot, 75005 Paris, France*

⁶ *Institute for Theoretical Physics and Astrophysics,*

University of Würzburg, Am Hubland 97074 Würzburg, Germany

⁷ *Russian Quantum Center, Skolokovo (Moscow), Russian Federation*

We study the relation between the microscopic properties of a many-body system and the electron spectra, experimentally accessible by photoemission. In a recent paper [Phys. Rev. Lett. **114**, 236402 (2015)], we introduced the “fluctuation diagnostics” approach, to extract the dominant wave vector dependent bosonic fluctuations from the electronic self-energy. Here, we first reformulate the theory in terms of fermionic modes, to render its connection with resonance valence bond (RVB) fluctuations more transparent. Secondly, by using a large- U expansion, where U is the Coulomb interaction, we relate the fluctuations to real space correlations. Therefore, it becomes possible to study how electron spectra are related to charge, spin, superconductivity and RVB-like real space correlations, broadening the analysis of an earlier work [Phys. Rev. B **89**, 245130 (2014)]. This formalism is applied to the pseudogap physics of the two-dimensional Hubbard model, studied in the dynamical cluster approximation. We perform calculations for embedded clusters with up to 32 sites, having three inequivalent \mathbf{K} -points at the Fermi surface. We find that as U is increased, correlation functions gradually attain values consistent with an RVB state. This first happens for correlation functions involving the antinodal point and gradually spreads to the nodal point along the Fermi surface. Simultaneously a pseudogap opens up along the Fermi surface. We relate this to a crossover from a Kondo-like state to an RVB-like localized cluster state and to the presence of RVB and spin fluctuations. These changes are caused by a strong momentum dependence in the cluster bath-couplings along the Fermi surface. We also show, from a more algorithmic perspective, how the time-consuming calculations in fluctuation diagnostics can be drastically simplified.

I. INTRODUCTION

The one-particle electronic spectrum is experimentally accessible, often with high accuracy, by means of photoemission and inverse photoemission spectroscopy.¹⁻³ While the spectral functions contain important information about the properties of the system, the extraction of this information is highly nontrivial. In fact, in the presence of strong correlations, different theoretical groups often obtain similar results for spectra, but draw different conclusions about the underlying physics. There is therefore a great need for reasonably unbiased methods for determining the physics from a spectral analysis. In particular, an important step would be to relate observable spectral properties to real space correlation functions and to momentum-dependent fluctuating modes.

Conceptually, we can think of the electron spectrum $\rho(\mathbf{k}, \varepsilon)$ in two quite different ways. Within a standard quantum many-body formalism, we can write

$$\rho(\mathbf{k}, \varepsilon) = -\frac{1}{\pi} \text{Im}g(\mathbf{k}, \varepsilon + i0^+) \quad (1)$$

$$g(\mathbf{k}, z) = \frac{1}{z + \mu - \varepsilon_{\mathbf{k}} - \Sigma(\mathbf{k}, z)},$$

where g is the Green’s function, Σ is the self-energy, \mathbf{k} is a wave vector, ε the energy and μ is the chemical potential. This representation emphasizes the role of the self-energy and it allows, by applying the “fluctuation diagnostics” approach⁴ to Σ , to identify the predominant fluctuating modes of the system.

Alternatively, using a more quantum-chemistry oriented point of view, we can express the spectral function also as

$$\rho(\mathbf{k}, \varepsilon) = \sum_n |\langle E_n(N-1) | c_{\mathbf{k}} | E_0(N) \rangle|^2 \quad (2)$$

$$\times \delta[\varepsilon - E_0(N) + E_n(N-1) + \mu].$$

This expression has for simplicity been written for zero temperature ($T = 0$) and $\varepsilon \leq 0$ (photoemission). Here $|E_0(N)\rangle$ is the initial (ground-)state for N electrons and $|E_n(N-1)\rangle$ is the n th excited final state for $N-1$ electrons, resulting in the photoemission process. $E_0(N)$ and $E_n(N-1)$ are the corresponding energies. This formalism tends to focus on the properties of the initial state, often described in terms of real space correlation functions, and how they influence the coupling to relevant final states. It therefore connects the spectra to ground-state properties in a natural way.

These two approaches provide two complementary views on the electronic spectra. In this paper, we describe how they work for theoretical calculations of strongly-correlated systems and how they are interconnected. In particular, we will show that ρ can be related either to momentum-dependent fluctuations or to real space correlation functions.

The spectra of strongly-correlated systems can be computed by means of different algorithms: lattice QMC,⁵ functional renormalization group,⁶ parquet approximation,⁷⁻⁹ and cluster extensions¹⁰ of the dynamical mean field theory (DMFT)^{11,12} such as the cellular-DMFT^{13,14} or the dynamical cluster approximation (DCA)¹⁵ as well as diagrammatic extensions¹⁶⁻²⁶ of DMFT.

The relation between the complementary views given by Eq. (1) and (2) will be illustrated using the example of the pseudogap²⁷ in the two-dimensional Hubbard model. Because of its relevance for the physics of high- T_c cuprates this problem has been extensively studied theoretically.²⁸⁻⁴³ In particular, the formation of the pseudogap has been ascribed to either spin^{28,30-32,35,36} or to superconducting fluctuations.³⁷⁻³⁹ It has also been argued that the pseudogap and superconductivity phases can compete.⁴¹⁻⁴³ The pseudogap is hence a perfect case of study where controversial interpretations of spectral properties can arise.

The interpretation of the pseudogap physics within the many-body framework of Eq. (1) has recently been discussed in Ref. 4 using the “fluctuation diagnostics” approach. Within this scheme, the self-energy Σ is first expressed, through the Schwinger-Dyson equation of motion (EOM), in terms of a two-particle scattering amplitude F . The EOM is then written in different representations, corresponding to the different scattering channels (charge, spin and particle-particle). This way, it has been shown that spin fluctuations with $\mathbf{Q} = (\pi, \pi)$ gives the dominant ($\sim 75\%$) contribution to Σ , while pairing fluctuations do not contribute much for unconventional (non s -wave) superconductors. Such precise quantification has been possible by performing partial summations over the internal fermionic frequencies and momenta of the EOM, and by comparing the different terms of the partial sum in the complementary representations.

While this approach provides us with a clear-cut “diagnostics” of the dominant fluctuations, it does not explain *why* they become large for given values of the Coulomb interaction U and certain momenta. Moreover, it does also not explain the reason for the strong momentum (\mathbf{K}) differentiation of Σ occurring in the hole-doped region of the phase diagram of the two-dimensional Hubbard model.

A rather different approach, in fact closer to the spirit of Eq. (2), was taken by Ferrero *et al.*,⁴⁴ De Leo *et al.*,⁴⁵ and Capone *et al.*,⁴⁶ who considered two- and three-orbital Anderson models and a four-impurity model. Their work focuses on changes of the initial state, emphasizing the crossover from a Kondo-screened to an

unscreened state. For the case of the A_3C_{60} ($A = K, Rb$) compounds, they linked the appearance of a spectral pseudogap to an unscreened ground state. In these works, the strong \mathbf{K} dependence of the pseudogap, such as that of the cuprates, was however not addressed.

A similar formalism has been developed for analyzing the pseudogap in cuprates, and in particular its momentum dependence.⁴⁷ For a small Coulomb interaction and for an eight site embedded cluster in the DCA, it was found that cluster levels with the cluster momenta $\mathbf{K} = (\pi, 0)$, $(0, \pi)$ and $(\pm\pi/2, \pm\pi/2)$ each forms a Kondo-like state with its bath. As U is increased, the energy gain from the Kondo-like coupling is reduced and it becomes favorable to correlate (localize) electrons in the space of the $(\pi, 0)$ and $(0, \pi)$ cluster levels, due to the energy gained when these levels form a localized state on the cluster.⁴⁷ At this point a pseudogap forms for $\mathbf{K} = (\pi, 0)$ and $(0, \pi)$, due to the nondegenerate character of the localized state formed.⁴⁷ Due to the stronger coupling to the bath, the $\mathbf{K} = (\pm\pi/2, \pm\pi/2)$ levels at first stay mainly Kondo-like.⁴⁷ A further increase of U , however, eventually leads to a localization also of these levels, and the formation of a resonance valence bond⁴⁹ (RVB)-like state involving these levels and the $(\pi, 0)$ and $(0, \pi)$ levels. This then leads to a pseudogap also for $\mathbf{K} = (\pm\pi/2, \pm\pi/2)$.⁴⁷ While this approach gives insights into the structure of the ground-state correlations, in contrast to the fluctuation diagnostics, it does not provide a direct information about which fluctuations are important.

The purpose of this paper is hence to merge the approach of Ref. 4 with that of Ref. 47, and to clarify the intrinsic connection among the different results previously obtained by studying the physical mechanisms at work in the pseudogap phase. In order to make the link between the two schemes, it is convenient to first reformulate the “fluctuation diagnostics” of Ref. 4 in terms of fermionic modes. Technically, this corresponds to performing the partial summation in the EOM over the bosonic momenta and frequencies arriving at a decomposition of the self-energy in terms of fermionic contributions, rather than in terms of bosonic collective modes. In a second step, we will make a large- U approximation, which allows us to relate the bosonic- or fermionic-resolved fluctuations to real space correlations, e.g., charge, spin, superconductivity or RVB-like correlations.⁴⁹

The work presented here has both physical and algorithmic implications. In particular, the importance of RVB-like correlations found here as well as in Ref. 47 is *not* in contradiction to the importance of antiferromagnetic spin fluctuations found in Ref. 4. The formation of RVB-like correlations also leads to substantial spin correlations,^{47,48} which via the large U approximation introduced here, can be related to spin fluctuations.

On the numerical side, changing the order in performing the partial internal summations of the EOM represents a strong reduction of the numerical effort of both the “original” (bosonic) fluctuation diagnostics of Ref. 4

as well as of the calculations presented in this paper, because some of the frequency sums can then be performed analytically.

In Sec. II we present the methods and models. In Sec. III we develop the formalism. We give the relations between the vertex function and the self-energy and show how the self-energy can be related to real space correlations by making a large U approximation. In Sec. IV correlation functions for the RVB-like state in isolated clusters are discussed. Finally, Sec. V shows the relations between spectra and correlation functions. The results are summarized in Sec. VI.

II. METHODS AND MODELS

We use the dynamical cluster approximation (DCA)¹⁰ for calculating the self-energy, correlation functions and generalized susceptibilities. A cluster with N_c sites is embedded in a self-consistent bath. We consider $N_c = 4, 8$ and 32 . The cluster problem is solved using the Hirsch-Fye⁵⁰ method. For the cases considered here there is no sign problem, which allows us to calculate the various quantities with a rather good statistical accuracy.

For most of the work here we use the two-dimensional Hubbard model. This model is described by the Hamiltonian

$$H = t \sum_{\langle ij \rangle, \sigma} (c_{i\sigma}^\dagger c_{j\sigma} + c_{j\sigma}^\dagger c_{i\sigma}) - \mu \sum_{i\sigma} n_{i\sigma} + U \sum_i n_{i\uparrow} n_{i\downarrow} \equiv H_0 + H_U, \quad (3)$$

where $\langle ij \rangle$ limits the sum to nearest neighbors, σ is a spin index and $n_{i\sigma} = c_{i\sigma}^\dagger c_{i\sigma}$. The nearest neighbor hopping integral is t , the on-site Coulomb interaction is given by U and we assume a square lattice. Typically a one-particle term

$$n_0 U \sum_{i\sigma} n_{i\sigma} \quad (4)$$

is added to H_0 and subtracted from H_U , where n_0 is an estimate of the occupancy per spin. This model is often used to describe cuprates superconductors.^{51,52} We use values of $U \sim (4-8)|t|$, which includes the range where a pseudogap occurs. The Coulomb interaction can also be expressed in reciprocal space

$$H_U = \frac{U}{N_c} \sum_{\mathbf{K}_1, \mathbf{K}_2, \mathbf{Q}} c_{\mathbf{K}_1\uparrow}^\dagger c_{\mathbf{K}_1+\mathbf{Q}\uparrow} c_{\mathbf{K}_2+\mathbf{Q}\downarrow}^\dagger c_{\mathbf{K}_2\downarrow}. \quad (5)$$

Cuprates show a pseudogap around $\mathbf{K} = (\pi, 0)$ and $(0, \pi)$ for moderate doping. As the doping is reduced, the pseudogap extends over a larger range of \mathbf{K} -values around the Fermi surface. A similar effect is seen at half-filling as U is increased.^{47,53} Here we therefore work at half-filling and vary U . This has the advantage that there is no sign problem, which makes it possible to study (DCA) clusters up to $N_c = 32$.

To improve our physical interpretation, below we also introduce a four-level model, which can be viewed as a simplified version of the $N_c = 4$ case. The model is particularly transparent and it can be analyzed in great detail. We discuss the cluster in terms of the different \mathbf{K} -states. The Coulomb part can be written in the form

$$H_U = U_{xx} \sum_{\mathbf{K}} n_{\mathbf{K}\uparrow} n_{\mathbf{K}\downarrow} + U_{xy} \sum_{\mathbf{K} \neq \mathbf{K}'} n_{\mathbf{K}\uparrow} n_{\mathbf{K}'\downarrow} \quad (6) \\ + J \sum_{\mathbf{K} \neq \mathbf{K}'} c_{\mathbf{K}\uparrow}^\dagger c_{\mathbf{K}'\downarrow}^\dagger c_{\mathbf{K}\downarrow} c_{\mathbf{K}'\uparrow} + J \sum_{\mathbf{K} \neq \mathbf{K}'} c_{\mathbf{K}\uparrow}^\dagger c_{\mathbf{K}\downarrow}^\dagger c_{\mathbf{K}'\downarrow} c_{\mathbf{K}'\uparrow},$$

where the first two terms describe the direct Coulomb interaction and the following two are exchange terms. For the Hubbard model $U_{xx} = U_{xy} = J = U/N_c$, as given in Eq. (5). For the $N_c = 4$ case, the orbitals $\mathbf{K} = (\pi, 0)$ and $(0, \pi)$ are particularly important for the physics, since at half-filling they are at the chemical potential. Therefore, in building up our simplified model, we consider a Hamiltonian where only these two orbitals are included, while the mainly occupied orbital $\mathbf{K} = (0, 0)$ as well as the mainly unoccupied $\mathbf{K} = (\pi, \pi)$ orbital are neglected. The two orbitals $\mathbf{K} = (\pi, 0)$ and $(0, \pi)$ are connected to one bath orbital each, giving a four-level model. The level structure of the isolated cluster containing just the $(\pi, 0)$ and $(0, \pi)$ levels can be fitted to the level structure of four isolated sites, relevant for the $N_c = 4$ calculation. We then find that U_{xx} has to be chosen slightly smaller than U_{xy} .⁴⁷ To simulate the $N_c = 4$ calculation we then choose

$$U_{xx} = U - \Delta U, \quad U_{xy} = U + \Delta U, \quad J = U. \quad (7)$$

Here we have redefined U ($U/N_c \rightarrow U$) to simplify the notations. Eq. (7) violates rotational invariance in spin-space and this is the price to be paid for simulating a four-site cluster with two levels. We use a very small ΔU and therefore this violation is small.

For the four-level model we introduce the following one-particle Hamiltonian

$$H_0 = (\varepsilon_c - \mu) \sum_{i=1}^2 \sum_{\sigma} n_{i\sigma} + (\varepsilon_b - \mu) \sum_{i=1}^2 \sum_{\sigma} n_{i\sigma} \\ + \sum_{i\sigma} V (c_{i\sigma}^\dagger c_{ib\sigma} + c_{ib\sigma}^\dagger c_{i\sigma}). \quad (8)$$

where c refers to cluster levels and b to bath levels. We use the Coulomb interaction in Eq. (6), where \mathbf{K} now runs over two levels ($i = 1, 2$), describing $\mathbf{K} = (\pi, 0)$ and $(0, \pi)$ respectively.

Although the $N_c = 4$ case is simulated by $\Delta U > 0$, we also consider $\Delta U < 0$. The change from $\Delta U > 0$ to $\Delta U < 0$ leads, in fact, to a dramatic change of the ground-state and of the spectral function. This illustrates nicely how the spectral function can provide important information about the ground-state.

As we already mentioned, the coupling of the embedded cluster to the bath plays an important role, and

TABLE I: Sum rule $-(1/\pi) \int \text{Im}\Gamma(\mathbf{K}, \varepsilon + i0^+)d\varepsilon$ according to Eq. (10) for different values of \mathbf{K} and N_c and for $t = -0.25$.

\mathbf{K}	Sum rule	
	$N_c = 8$	$N_c = 32$
$(\pi, 0)$	0.033	0.002
$(3\pi/4, \pi/4)$		0.025
$(\pi/2, \pi/2)$	0.149	0.047

therefore we discuss this here in a more general fashion. The noninteracting Green's function can be written as

$$g_0(\mathbf{K}, i\nu_n) \equiv [i\nu_n - \Delta - \bar{\varepsilon}_{\mathbf{K}} - \Gamma_{\mathbf{K}}(i\nu_n)]^{-1}, \quad (9)$$

where ν_n is a Matsubara frequency, $\Delta = n_0U - \mu$ and n_0 was defined below Eq. (4). Here the \mathbf{k} -space has been divided in N_c patches around each cluster \mathbf{K} -vector, where each patch contains \tilde{N} \mathbf{k} states. We define $\bar{\varepsilon}_{\mathbf{K}} = \frac{1}{\tilde{N}} \sum_{\tilde{\mathbf{k}}} \varepsilon_{\mathbf{K}+\tilde{\mathbf{k}}}$. The hybridization function Γ satisfies an important sum rule⁵⁴

$$-\frac{1}{\pi} \int \text{Im}\Gamma_{\mathbf{K}}(\varepsilon + i0^+)d\varepsilon = \frac{1}{\tilde{N}} \sum_{\tilde{\mathbf{k}}} (\varepsilon_{\mathbf{K}+\tilde{\mathbf{k}}} - \bar{\varepsilon}_{\mathbf{K}})^2, \quad (10)$$

where $\Gamma_{\mathbf{K}}(i\nu_n)$ has been analytically continued to real ε and 0^+ is an infinitesimal positive number. This result shows that the second moment of the $\varepsilon_{\mathbf{k}}$ inside a patch is a measure of the coupling to the bath. Due to the weak dispersion around $\mathbf{K} = (\pi, 0)$, $|\text{Im}\Gamma_{\mathbf{K}}(i\nu_n)|$ is much smaller for $(\pi, 0)$ than for $(\pi/2, \pi/2)$. The corresponding values are reported in Table I for $N_c = 8$ and 32. For $N_c = 8$ the difference is about a factor of four and for $N_c = 32$ the difference is even larger. In the latter case the patch around $\mathbf{K} = (\pi, 0)$ is very small and dominated by the saddle point for this \mathbf{K} .

III. FORMALISM AND DERIVATIONS

A. Two-particle vertex function

We first introduce generalized susceptibilities in the Matsubara formalism for a finite temperature $T = 1/\beta$. We follow the notations of Rohringer *et. al.*⁵⁵.

$$\begin{aligned} \chi_{\sigma\sigma'}(k; k'; q) &= \int_0^\beta d\tau_1 \int_0^\beta d\tau_2 \int_0^\beta d\tau_3 \\ &\times e^{-i[\nu\tau_1 - (\omega + \nu)\tau_2 + (\omega + \nu')\tau_3]} \\ &\times \langle T_\tau [c_{\mathbf{k}\sigma}^\dagger(\tau_1) c_{\mathbf{k}+\mathbf{q}\sigma}(\tau_2) c_{\mathbf{k}'+\mathbf{q}\sigma'}^\dagger(\tau_3) c_{\mathbf{k}'\sigma'}] \rangle \\ &- \beta g_\sigma(k) g_{\sigma'}(k') \delta_{q=0}. \end{aligned} \quad (11)$$

Here we use the condensed notations $q = (\mathbf{Q}, \omega)$ and $k = (\mathbf{K}, \nu)$, where \mathbf{Q} and \mathbf{K} are (cluster) wave vectors and ω and ν are Matsubara boson and fermion frequencies, respectively. The Green's function is given by

$$g_\sigma(k) = - \int_0^\beta d\tau e^{i\nu\tau} \langle c_{\mathbf{K}\sigma}(\tau) c_{\mathbf{K}\sigma}^\dagger \rangle, \quad (12)$$

where $c_{\mathbf{K}\sigma}^\dagger$ creates an electron with the wave vector \mathbf{K} and spin σ and $\langle \dots \rangle$ is the thermodynamical average. From χ we obtain the full vertex F

$$\begin{aligned} \chi_{\sigma\sigma'}(k; k'; q) &= -\beta g_\sigma(k) g_{\sigma'}(k+q) \delta_{kk'} \delta_{\sigma\sigma'} \\ &- g_\sigma(k) g_{\sigma'}(k+q) F_{\sigma\sigma'}(k; k'; q) g_{\sigma'}(k') g_{\sigma'}(k'+q). \end{aligned} \quad (13)$$

In the SU(2) symmetric cases considered here, g is independent of σ ($g = g_\uparrow = g_\downarrow$), and the index σ is therefore dropped in the following. The self-energy Σ can be obtained from the equation of motion. For the Hubbard model [Eqs. (3, 5)] we have

$$\Sigma(k) = [g(k)]^{-1} \int_0^\beta \langle [H_U(\tau), c_{\mathbf{K}\sigma}(\tau)] c_{\mathbf{K}\sigma}^\dagger \rangle d\tau e^{i\nu\tau}. \quad (14)$$

The commutator can be expressed in terms of the vertex function F , leading to the Schwinger-Dyson equation

$$\begin{aligned} \Sigma(k) - \left(\frac{n}{2} - n_0\right)U \\ = -\frac{U}{\beta^2 N_c} \sum_{k', q} F_{\uparrow\downarrow}(k, k', q) g(k') g(k'+q) g(k+q) \end{aligned} \quad (15)$$

where N_c is the number of \mathbf{K} -points in the embedded cluster.

Exploiting the SU(2) symmetry of the Hubbard model for the paramagnetic state⁵⁵ and ‘‘crossing relations’’,⁵⁵ due to the electrons being identical particles, specific identities between different vertex functions can be derived. By means of these relations Eq. (15) can be rewritten as⁴

$$\begin{aligned} \Sigma(k) - \left(\frac{n}{2} - n_0\right)U \\ = \frac{U}{\beta^2 N_c} \sum_{k', q} F_{sp}(k, k'; q) g(k') g(k'+q) g(k+q), \\ = -\frac{U}{\beta^2 N_c} \sum_{k', q} F_{ch}(k, k'; q) g(k') g(k'+q) g(k+q), \\ = -\frac{U}{\beta^2 N_c} \sum_{k', q} F_{pp}(k, k'; q) g(k') g(q-k') g(q-k), \end{aligned} \quad (16)$$

where

$$\begin{aligned} F_{ch}(k; k'; q) &= F_{\uparrow\uparrow}(k; k'; q) + F_{\uparrow\downarrow}(k; k'; q) \\ F_{sp}(k; k'; q) &= F_{\uparrow\uparrow}(k; k'; q) - F_{\uparrow\downarrow}(k; k'; q) \\ F_{pp}(k; k'; q) &= F_{\uparrow\downarrow}(k; k'; q) - F_{\downarrow\downarrow}(k; k'; q) \end{aligned} \quad (17)$$

The three equations in Eq. (16) are all exact and give identical results if the summations are performed until convergence. Using the scheme coined ‘‘fluctuation diagnostics’’,⁴ the partial contribution to these sums were studied as a function of q .^{4,56} In particular, we recall that if there are low-lying spin fluctuations for $\mathbf{Q} = \mathbf{Q}_0$, these give large contributions in the top formula in Eq. (16) for $\mathbf{Q} = \mathbf{Q}_0$ and small ω . In the other two formulas, on the other hand, the contributions are spread out over

many \mathbf{Q} and ω . In a similar way, one can detect the presence of well defined charge and superconductivity fluctuations from the second and third formula, respectively. This makes it possible to identify which fluctuations are important in determining a given numerical result for the self-energy. From the algorithmic point of view, it is important to recall that the advantage of this procedure w.r.t. a more direct decomposition⁵⁷ of the self-energy in terms of the parquet equations,⁵⁸ is to avoid, at any step of the algorithm, the calculations of possibly divergent^{59–68} two-particle irreducible vertex functions.

Complementarily to the fluctuation diagnostics, in Ref. 47 the correlation function

$$L(\mathbf{K}) = \langle n_{\mathbf{K}\uparrow} n_{\mathbf{K}\downarrow} \rangle - \langle n_{\mathbf{K}\uparrow} \rangle \langle n_{\mathbf{K}\downarrow} \rangle. \quad (18)$$

was introduced to relate the spectral function to the underlying ground-state properties. This correlation function describes the transition from a Kondo-like state to localized state on the cluster. For small U , the Kondo screening of the different \mathbf{K} states is important, as discussed in the introduction. We then obtained $L < 0$, showing the beginning of the formation of a spin 1/2 state in the orbital \mathbf{K} . This spin state was found to couple antiferromagnetically to the bath, leading to a Kondo-like state. For larger values of U , it was found that localized states form on the cluster, e.g., for $N_c = 4$ as in Eq. (43) below. This leads to $L > 0$. We will use this correlation function later, to clarify the relation between the results obtained by means of the fluctuation diagnostics and the complementary approach of Ref. 47.

B. Relation to susceptibilities

In this subsection, we start by reformulating the fluctuation diagnostic approach of Ref. 4 in terms of fermionic modes. This reformulation is, from a physically point of view, rigorously equivalent to the bosonic one of Ref. 4 for the case of SU(2)-symmetric models mostly considered in this work. It allows however, to establish in a more immediate way the connection between the predominant fluctuations and the underlying correlations in real space.

To this aim, we will introduce an extended set of correlation functions designed to capture the complementary aspects of the underlying physics. In particular, going beyond the derivations of Ref. 4, we will also study the \mathbf{K}' dependence of the two-particle correlation function after a summation over the transfer momentum \mathbf{Q} has been performed, as there the connection to RVB-like correlations is more easily visible. At the same time, we will discuss how the extended formalism allows for a drastic numerical simplification of the formulas previously used in fluctuation diagnostics.⁴

The fermionic reformulation of the equation of Ref. 4 is readily obtained by following an alternative route in treating the equation of motion. This corresponds, in

practice, to the situation in which the frequency summations in Eqs. (15, 16) have already been performed. From Eq. (13), we can see that the susceptibility is the vertex function $F_{\uparrow\downarrow}$ times four Green's functions, while the contribution to the self-energy is $F_{\uparrow\downarrow}$ times three Green's functions. The derivation below essentially replaces the vertex function by the susceptibility divided by a Green's function and with two frequency summations performed.

As for the derivation, we start by inserting the expression of the Hubbard interaction in the commutator in Eq. (14), obtaining

$$\begin{aligned} \Sigma(k) + n_0 U &= -\frac{U}{N_c g(k)} \sum_{\mathbf{K}'\mathbf{Q}} \quad (19) \\ &\times \int_0^\beta d\tau e^{i\nu\tau} \langle c_{\mathbf{K}+\mathbf{Q}\uparrow}(\tau) c_{\mathbf{K}'+\mathbf{Q}\downarrow}^\dagger(\tau) c_{\mathbf{K}'\downarrow}(\tau) c_{\mathbf{K}\uparrow}^\dagger \rangle. \end{aligned}$$

We now introduce a specific two-particle correlation function

$$\begin{aligned} A_{\sigma\sigma'}(\mathbf{K}, \mathbf{K}', \mathbf{Q}) \quad (20) \\ &= -\frac{U}{N_c} \int_0^\beta d\tau e^{i\nu\tau} \langle c_{\mathbf{K}+\mathbf{Q}\sigma}(\tau) c_{\mathbf{K}'+\mathbf{Q}\sigma'}^\dagger(\tau) c_{\mathbf{K}'\sigma'}(\tau) c_{\mathbf{K}\sigma}^\dagger \rangle \\ &= \frac{U}{N_c} \int_0^\beta d\tau e^{-i\nu\tau} \langle c_{\mathbf{K}\sigma}^\dagger(\tau) c_{\mathbf{K}+\mathbf{Q}\sigma} c_{\mathbf{K}'+\mathbf{Q}\sigma'}^\dagger c_{\mathbf{K}'\sigma'} \rangle, \end{aligned}$$

and express Eq. (19) in terms of $A_{\uparrow\downarrow}(\mathbf{K}, \mathbf{K}', \mathbf{Q})$. In the following we focus on the lowest Matsubara fermion frequency ($\nu = \pi/\beta$) only; this frequency will therefore not be shown explicitly in the corresponding notation for $A_{\uparrow\downarrow}(\mathbf{K}, \mathbf{K}', \mathbf{Q})$. Comparing with Eqs. (13, 15), we can see that the integral in Eq. (19, 20) corresponds, to a large extent, to the susceptibility $\chi_{\uparrow\downarrow}(k, k', q)$ summed over the frequencies ν' and ω :

$$\begin{aligned} \Sigma(k) + n_0 U &= \quad (21) \\ &= \frac{1}{g(k)} \sum_{\mathbf{K}'\mathbf{Q}} \frac{U}{\beta^2 N_c} \sum_{\nu'\omega} \left[\chi_{\uparrow\downarrow}(k, k', q) + \frac{N_c n}{2} g(k) \delta_{\mathbf{Q}\mathbf{0}} \right] \\ &= \frac{1}{g(k)} \sum_{\mathbf{K}'\mathbf{Q}} A_{\uparrow\downarrow}(\mathbf{K}, \mathbf{K}', \mathbf{Q}) \end{aligned}$$

Since all frequency summations have already been performed in Eq. (22), this expression is much easier to calculate than the corresponding terms appearing in Eq. (16). It is important to stress that this represents a *significant advantage* for the algorithms based on partial summation of the EOM, making it possible, e.g., to perform the fluctuation diagnostics of the DCA self-energy for much larger clusters ($N_c = 32$) than before ($N_c = 8$).

Note that in Eq. (13) a Hartree term was separated out, while it is kept in the definition of $A_{\uparrow\downarrow}$ in Eq. (20), making $A_{\uparrow\downarrow}/g$ slightly different from $F_{\uparrow\downarrow} g g g$. Similarly, $A_{\uparrow\uparrow}/g$ differs by a constant term from $F_{\uparrow\uparrow} g g g$. However, in this work we consider a half-filled system and \mathbf{K} at the Fermi surface. For this case $g(k)$ is imaginary, and

the difference in definition shows up in the imaginary part only. Hence, since we are mostly interested in the imaginary part of Σ at the Fermi level, we can focus on $\text{Re } A_{\sigma\sigma'}$ only, for which the difference between $A_{\uparrow\downarrow}/g$ and $F_{\uparrow\downarrow}ggg$ is of no particular interest.

In order to rationalize the different, complementary treatments of the EOM discussed in this work, we introduce the following correlation functions:

$$\begin{aligned} B_{\sigma\sigma'}(\mathbf{K}, \mathbf{K}') &= \sum_{\mathbf{Q}} A_{\sigma\sigma'}(\mathbf{K}, \mathbf{K}', \mathbf{Q}) \\ C_{\sigma\sigma'}(\mathbf{K}, \mathbf{Q}) &= \sum_{\mathbf{K}'} A_{\sigma\sigma'}(\mathbf{K}, \mathbf{K}', \mathbf{Q}) \\ D_{\sigma\sigma'}(K) &+ n_0 U g(k) \\ &= \sum_{\mathbf{K}'} B_{\sigma\sigma'}(\mathbf{K}, \mathbf{K}') = \sum_{\mathbf{Q}} C_{\sigma\sigma'}(\mathbf{K}, \mathbf{Q}), \end{aligned} \quad (22)$$

that correspond to different ways of realizing the fluctuation diagnostics. In fact, while C is the quantity defined in the original fluctuation diagnostics algorithm where partial summations of all internal variables, but the transfer momentum \mathbf{Q} , have been performed. B corresponds to an equivalent scheme, where all internal variables are summed, except the (incoming/outgoing) electron momentum \mathbf{K}' . This latter procedure can be, thus viewed as a “fermionic” reformulation of the fluctuation diagnostics. Finally, the quantity D is obtained performing the residual summation in the definition of B and C , and it depends, thus, only on the external variables (here: on the momentum \mathbf{K}).

By exploiting these definitions, we can rewrite Eq. 22 in several equivalent ways:

$$\begin{aligned} \Sigma(k) + n_0 U &= \frac{1}{g(k)} \sum_{\mathbf{K}'\mathbf{Q}} A_{\uparrow\downarrow}(\mathbf{K}, \mathbf{K}', \mathbf{Q}) \\ &= \frac{1}{g(k)} \sum_{\mathbf{K}'} B_{\uparrow\downarrow}(\mathbf{K}, \mathbf{K}') \\ &= \frac{1}{g(k)} \sum_{\mathbf{Q}} C_{\uparrow\downarrow}(\mathbf{K}, \mathbf{Q}) \\ &= \frac{1}{g(k)} D_{\uparrow\downarrow}(\mathbf{K}) + n_0 U. \end{aligned} \quad (23)$$

The Green’s function given in Eq. (1) can be written as

$$g(k) = [i\nu_n - \Delta - \varepsilon_{\mathbf{K}} - \Sigma(k)]^{-1}, \quad (24)$$

Then we have

$$\Sigma(k) = [i\nu_n - \Delta - \varepsilon_{\mathbf{K}}] \frac{D_{\uparrow\downarrow}(\mathbf{K})}{1 + D_{\uparrow\downarrow}(\mathbf{K})}. \quad (25)$$

From this expression, we see immediately that $D \rightarrow -1$ leads to a singularity, thus for $D \approx -1$ the system may become a non Fermi liquid or a Mott insulator.

Performing the τ integration in Eq. (20), and exploit-

ing the Lehmann representation, we obtain

$$\begin{aligned} A_{\sigma\sigma'}(\mathbf{K}, \mathbf{K}', \mathbf{Q}) &= \frac{U}{N_c Z} \sum_{mnn} \frac{e^{-\beta \tilde{E}_m(N+1)} + e^{-\beta \tilde{E}_n(N)}}{i\nu + \tilde{E}_n(N) - \tilde{E}_m(N+1)} \\ &\times \langle n | c_{\mathbf{K}+\mathbf{Q}\sigma} c_{\mathbf{K}'+\mathbf{Q}\sigma'}^\dagger c_{\mathbf{K}'\sigma'} | m \rangle \langle m | c_{\mathbf{K}\sigma}^\dagger | n \rangle, \end{aligned} \quad (26)$$

where $\tilde{E}_n(N) = E_n(N) - \mu N$.

To simplify this expression, we now assume that β is very large and that

$$\begin{aligned} \beta[\tilde{E}_1(N_{\text{el}}) - \tilde{E}_0(N_{\text{el}})] &\gg 1 \\ \beta[\tilde{E}_1(N_{\text{el}} \pm 1) - \tilde{E}_0(N_{\text{el}} \pm 1)] &\gg 1 \\ \beta[\tilde{E}_0(N_{\text{el}} \pm 1) - \tilde{E}_0(N_{\text{el}})] &\gg 1, \end{aligned} \quad (27)$$

Here N_{el} is the number of electrons which minimizes $\tilde{E}_0(N)$. For a very large and positive value of U at half-filling, we have approximately that $E_n(N_{\text{el}} - 1)O(U^0)$, $E_n(N_{\text{el}}) = O(U^0)$, $E_n(N_{\text{el}} + 1) = U + O(U^0)$ and $\mu = U/2$. Similarly, for a very large, negative U at half-filling, we have approximately that $E_n(N_{\text{el}} - 1) = (N_{\text{el}}/2 - 1)U$, $E_n(N_{\text{el}}) = (N_{\text{el}}/2)U$, $E_n(N_{\text{el}} + 1) = (N_{\text{el}}/2)U$ and $\mu = U/2$.

In both cases, we obtain:

$$\tilde{E}_n(N_{\text{el}} \pm 1) - \tilde{E}_0(N_{\text{el}}) = \frac{|U|}{2} + O(U^0). \quad (28)$$

Within the assumptions in Eq. (27) we have, furthermore, that

$$Z = e^{-\beta \tilde{E}_0(N_{\text{el}})}, \quad (29)$$

because all other contributions to Z can be neglected and we can also neglect the corresponding exponents in Eq. (20). We have, thus, two types of contributions: i) $|n\rangle$ is the lowest (N_{el}) state and $|m\rangle$ is any ($N_{\text{el}} + 1$) state or ii) $|m\rangle$ is the lowest (N_{el}) state and $|n\rangle$ is any ($N_{\text{el}} - 1$) state. As anticipated, we consider the lowest Matsubara frequency only, and assume that $\pi/\beta \ll |U|/2$, so that ν can be neglected. Inserting Eq. (28) in Eq. (26), we obtain

$$\begin{aligned} A_{\sigma\sigma'}(\mathbf{K}, \mathbf{K}', \mathbf{Q}) &= \frac{4}{N_c} \frac{U}{|U|} \langle E_0(N_{\text{el}}) | c_{\mathbf{K}\sigma}^\dagger c_{\mathbf{K}+\mathbf{Q}\sigma} c_{\mathbf{K}'+\mathbf{Q}\sigma'}^\dagger c_{\mathbf{K}'\sigma'} | E_0(N_{\text{el}}) \rangle \\ &- \frac{2}{N_c} \frac{U}{|U|} \langle E_0(N_{\text{el}}) | c_{\mathbf{K}'\sigma'}^\dagger c_{\mathbf{K}'\sigma'} | E_0(N_{\text{el}}) \rangle \delta_{\mathbf{Q}=(0,0)} \\ &- \frac{2}{N_c} \frac{U}{|U|} \langle E_0(N_{\text{el}}) | c_{\mathbf{K}+\mathbf{Q}\sigma} c_{\mathbf{K}+\mathbf{Q}\sigma}^\dagger | E_0(N_{\text{el}}) \rangle \delta_{\mathbf{K}\mathbf{K}'} \delta_{\sigma\sigma'} \end{aligned} \quad (30)$$

For the following discussion, it is useful to sum the first expectation value in Eq. (30) over \mathbf{K}' and transformed

to real space, expressing $c_{\mathbf{K}\sigma}$ in the quantities $c_{\mathbf{R}\sigma}$.

$$\begin{aligned}
& \sum_{\mathbf{K}'} \langle E_0(N_{el}) | c_{\mathbf{K}\sigma}^\dagger c_{\mathbf{K}+\mathbf{Q}\sigma} c_{\mathbf{K}'+\mathbf{Q}\sigma'}^\dagger c_{\mathbf{K}'\sigma'} | E_0(N_{el}) \rangle \\
&= \frac{1}{N_c} \sum_{\mathbf{R}_1 \mathbf{R}_2 \mathbf{R}_3} e^{i[\mathbf{K}\cdot(\mathbf{R}_1-\mathbf{R}_2)+\mathbf{Q}\cdot(\mathbf{R}_3-\mathbf{R}_2)]} \\
&\times \langle E_0(N_{el}) | c_{\mathbf{R}_1\sigma}^\dagger c_{\mathbf{R}_2\sigma} c_{\mathbf{R}_3\sigma'}^\dagger c_{\mathbf{R}_3\sigma'} | E_0(N_{el}) \rangle \\
&\simeq \frac{1}{N_c} \sum_{\mathbf{R}_1 \mathbf{R}_2} e^{i\mathbf{Q}\cdot(\mathbf{R}_2-\mathbf{R}_1)} \\
&\times \langle E_0(N_{el}) | n_{\mathbf{R}_1\sigma} n_{\mathbf{R}_2\sigma'} | E_0(N_{el}) \rangle
\end{aligned} \tag{31}$$

Note that the last equation is obtained by neglecting the double occupied/empty (singly occupied) states, consistent with the large positive (negative) interaction regime considered here. These large U approximations, the assumption in Eq. (28) and the neglect of double occupancy, have been discussed in Appendix B.

We now perform the \mathbf{K}' and \mathbf{Q} summations over $A_{\uparrow\downarrow}$.

$$\begin{aligned}
D_{\uparrow\downarrow}(\mathbf{K}) + n_0 U g(k) &= \sum_{\mathbf{K}'\mathbf{Q}} A_{\uparrow\downarrow}(\mathbf{K}, \mathbf{K}', \mathbf{Q}) \\
&= \frac{U}{|U|} \frac{4}{N_c} \sum_{\mathbf{R}_1} \langle E_0(N_{el}) | n_{\mathbf{R}_1\uparrow} n_{\mathbf{R}_1\downarrow} | E_0(N_{el}) \rangle \\
&- \frac{U}{|U|} \frac{2}{N_c} \sum_{\mathbf{K}'} \langle E_0(N_{el}) | n_{\mathbf{K}'\downarrow} | E_0(N_{el}) \rangle
\end{aligned} \tag{32}$$

For a half-filled system and a large positive U , the first term on the right hand side contributes nothing, while the second term contributes -1. For a large negative U the first term instead contributes -2 and the second term +1. In both cases the total contribution to $D_{\uparrow\downarrow}(\mathbf{K}) = -1$. In the same limit the sum rule for $A_{\uparrow\uparrow}$ is zero. For the half-filled case and for \mathbf{K} at the Fermi surface, the term $n_0 U g$ is zero to leading order in $1/U$, so that $D_{\uparrow\downarrow} \rightarrow -1$ and $D_{\uparrow\uparrow} \rightarrow 0$.

While the derivations of this section have been performed exploiting specific assumptions, we will show later that for large values of U they agree with numerical results calculated *without* these assumptions (see also Appendix B). Thus they provide a reasonable theoretical framework for the physical interpretation of our numerical data.

C. Relation to localized ground states

In Ref. 47 it has been argued that the progressive localization of some, and eventually of all, electrons on the embedded DCA cluster as U is increased, plays an important role for the formation of the pseudogap. In particular, for large U , it was found that the electrons on the cluster localize into an RVB state.

Below we discuss how the formulas [Eqs. (19, 20, 23, 30)] for the self-energy expressed in terms of the susceptibilities can be related to such a localization. In this

subsection we assume that $U > 0$. To this aim, we now switch to working in real space. Performing the summation over \mathbf{Q} in Eq. (30) we obtain

$$\begin{aligned}
B_{\uparrow\downarrow}(\mathbf{K}, \mathbf{K}', \nu) &= \sum_{\mathbf{Q}} A_{\uparrow\downarrow}(\mathbf{K}, \mathbf{K}', \mathbf{Q}) = \\
&- \frac{2}{N_c} \langle n_{\mathbf{K}'\downarrow} \rangle - \frac{4}{N_c^2} \sum_{\mathbf{R}_1 \neq \mathbf{R}_2} e^{i(\mathbf{K}-\mathbf{K}')\cdot(\mathbf{R}_1-\mathbf{R}_2)} \\
&\times \langle E_0(N_{el}) | c_{\mathbf{R}_2\downarrow}^\dagger c_{\mathbf{R}_2\uparrow} c_{\mathbf{R}_1\uparrow}^\dagger c_{\mathbf{R}_1\downarrow} | E_0(N_{el}) \rangle.
\end{aligned} \tag{33}$$

Here we have introduced similar approximations as in Eq. (31), assuming half-filling and a large U .

The operator in Eq. (33) couples to a valence bond

$$(12) = \frac{1}{\sqrt{2}} (c_{\mathbf{R}_1\uparrow}^\dagger c_{\mathbf{R}_2\downarrow}^\dagger - c_{\mathbf{R}_1\downarrow}^\dagger c_{\mathbf{R}_2\uparrow}^\dagger) | \text{vac} \rangle \tag{34}$$

between the sites \mathbf{R}_1 and \mathbf{R}_2 with the strength $-1/2$. Here $|\text{vac}\rangle$ is the vacuum state. For a nearest neighbor (NN) bond on a square lattice and $\mathbf{K} - \mathbf{K}' = (\pi, \pi)$ we then obtain a negative contribution due to the sign of the exponential, while for $\mathbf{K} - \mathbf{K}' = (0, 0)$ the contribution is positive.

For a square lattice we can divide the lattice in two sublattices A and B, where the nearest neighbor of a site in one sublattice belongs to the other sublattice. The NN-RVB is a superposition of singlets of the type of Eq. (34) between neighboring sites taken from A to B sublattice with equal positive bond amplitudes:

$$| \Psi_0 \rangle = \sum_{i_\alpha, j_\beta} (i_1 j_1) (i_2 j_2) \dots (i_n j_n) \tag{35}$$

where i_α (j_β) denote neighbor sites in the A-sublattice (B-sublattice) and $(i_\alpha j_\beta)$ denotes a singlet. First we only consider contributions where the operator in Eq. (33) acts within a given bond. For a NN-RVB state these contributions together with the term $-2 \langle n_{\mathbf{K}'\downarrow} \rangle / N_c$ gives a substantial negative result for $\mathbf{K} - \mathbf{K}' = (\pi, \pi)$, while there tends to be a net positive contribution for $\mathbf{K} = \mathbf{K}'$. In addition there are also contributions where the operator in Eq. (33) acts on a product of two bonds $(i_1 j_1) (i_2 j_2)$, i.e., the two-site operator acts on one site of each bond. Then we can get a contribution also from second nearest neighbor, even for a NN-RVB state. In this case the exponent in Eq. (33) takes the same value for both $\mathbf{K} - \mathbf{K}' = (\pi, \pi)$ and $\mathbf{K} - \mathbf{K}' = (0, 0)$, reducing the difference between these two cases. As we will show in the following, $B_{\uparrow\downarrow}(\mathbf{K}, \mathbf{K}')$ encodes, nevertheless, very clear signals of the RVB state formation.

Within the approximations above, the large U results (33) only depends on $\mathbf{K} - \mathbf{K}'$ and not on the two wave-vectors individually. For finite values of U , however, there is also a difference between $\mathbf{K} = (\pi, 0)$ and $\mathbf{K} = (\pi/2, \pi/2)$, which plays an important role in the interpretation of the results.

D. Relation to the “fluctuation diagnostics”

We now discuss the relation to “fluctuation diagnostics”⁴ introduced earlier. While for the SU(2)-symmetric case, this connection can be analytically derived from the exact relations holding between the correlation functions⁶⁹ B and C . Here we however provide a physically more explicit derivation. To this aim, we first consider the coupling to charge and spin fluctuations. For this purpose we introduce

$$C_{\text{ch/sp}}(\mathbf{K}, \mathbf{Q}) = \sum_{\mathbf{K}'} [A_{\uparrow\downarrow}(\mathbf{K}, \mathbf{K}', \mathbf{Q}) \pm A_{\uparrow\uparrow}(\mathbf{K}, \mathbf{K}', \mathbf{Q})] \quad (36)$$

and

$$\Sigma(k) = \sum_{\mathbf{Q}} C_{\text{ch/sp}}(\mathbf{K}, \mathbf{Q})/g(k). \quad (37)$$

Here we have used that $\sum_{\mathbf{K}'\mathbf{Q}} A_{\uparrow\uparrow}(\mathbf{K}, \mathbf{K}', \mathbf{Q}) = 0$.

The coupling to spin fluctuations is expected to be relevant for positive values of U . In particular, for large enough U , at half-filling, we have:

$$\begin{aligned} C_{\text{sp}}(\mathbf{K}, \mathbf{Q}) &= -\frac{2}{N_c^2} \sum_{\mathbf{R}_1 \mathbf{R}_2} e^{i\mathbf{Q}\cdot(\mathbf{R}_2-\mathbf{R}_1)} \quad (38) \\ &\times \langle E_0(N_{\text{el}}) | [n_{\mathbf{R}_1\uparrow} - n_{\mathbf{R}_1\downarrow}] [n_{\mathbf{R}_2\uparrow} - n_{\mathbf{R}_2\downarrow}] | E_0(N_{\text{el}}) \rangle \\ &+ \frac{2}{N_c} \langle E_0(N_{\text{el}}) | c_{\mathbf{K}+\mathbf{Q}\uparrow} c_{\mathbf{K}+\mathbf{Q}\uparrow}^\dagger | E_0(N_{\text{el}}) \rangle. \end{aligned}$$

One can then see that if neighboring sites have opposite spins a large (negative) contribution to C_{sp} is obtained for $\mathbf{Q} = (\pi, \pi)$. This is indeed perfectly consistent with the considerations made in the previous subsection due to an exact relation which can be derived in the SU(2)-symmetric case: $C_{\text{sp}}(\mathbf{K}, \mathbf{Q} = (\pi, \pi)) = B_{\uparrow\downarrow}(\mathbf{K}, \mathbf{K} + (\pi, \pi))$.

We next consider the coupling to charge fluctuations. These are expected to become important for negative U , and therefore we consider $U < 0$ below. In Eq. (30), $U/|U|$ then contributes an extra minus sign. Eq. (31) is still a good approximation for large U , but now because double occupancy is favored. We then have

$$\begin{aligned} C_{\text{ch}}(\mathbf{K}, \mathbf{Q}) &= -\frac{2}{N_c^2} \sum_{\mathbf{R}_1 \mathbf{R}_2} e^{i\mathbf{Q}\cdot(\mathbf{R}_2-\mathbf{R}_1)} \langle E_0(N_{\text{el}}) | \quad (39) \\ &\times [n_{\mathbf{R}_1\uparrow} + n_{\mathbf{R}_1\downarrow} - \langle n \>] [n_{\mathbf{R}_2\uparrow} + n_{\mathbf{R}_2\downarrow} - \langle n \>] | E_0(N_{\text{el}}) \rangle \\ &+ \frac{2}{N_c} \langle E_0(N_{\text{el}}) | c_{\mathbf{K}+\mathbf{Q}\uparrow} c_{\mathbf{K}+\mathbf{Q}\uparrow}^\dagger | E_0(N_{\text{el}}) \rangle \\ &+ 2(\langle n \rangle - \langle n \rangle^2) \delta_{\mathbf{Q}(0,0)}, \end{aligned}$$

where we have assumed that there is no net spin polarization. If there is a checkerboard type of charge order, there is a large negative contribution for $\mathbf{Q} = (\pi, \pi)$.

While Eqs. (16) makes contact to susceptibilities via Eq. (13), Eqs. (38, 39) make direct contact to static charge or spin correlations in real space. This connection is based on the approximation (28).

Finally, we consider the coupling to superconductivity fluctuations. As discussed in Ref. 4, the coupling to unconventional superconductivity is weak, and the coupling is primarily to s -wave superconductivity. In the Hubbard model, this is found for negative U . We then consider $U < 0$. To study superconductivity we define⁵⁵

$$\begin{aligned} C_{\text{pp}}(\mathbf{K}, \mathbf{Q}) &= \sum_{\mathbf{K}'} A_{\uparrow\downarrow}(\mathbf{K}, \mathbf{K}', \mathbf{Q} - \mathbf{K} - \mathbf{K}') \quad (40) \\ &= -\frac{4}{N_c^2} \sum_{\mathbf{R}_1 \mathbf{R}_2 \mathbf{R}_3} e^{i[\mathbf{K}\cdot(\mathbf{R}_1-\mathbf{R}_3) - \mathbf{Q}\cdot(\mathbf{R}_2-\mathbf{R}_3)]} \\ &\langle E_0(N_{\text{el}}) | c_{\mathbf{R}_1\uparrow}^\dagger c_{\mathbf{R}_3\downarrow}^\dagger c_{\mathbf{R}_2\downarrow} c_{\mathbf{R}_2\uparrow} | E_0(N_{\text{el}}) \rangle \\ &+ \langle n \rangle \delta_{\mathbf{Q}(0,0)} \end{aligned}$$

We are interested in the $\mathbf{Q} = (0, 0)$ contribution. The contribution in the sum in Eq. (40) for $\mathbf{R}_3 = \mathbf{R}_1$ is then particularly important, since the exponential function is then unity. The coupling to s -wave superconductivity is then strong.

Using Eq. (22), we can see that a spin density wave contributes to $D \rightarrow -1$ in Eq. (38). The same is true for a charge density wave in Eq. (39) and a s -wave superconductivity pairing in Eq. (40). In all three cases this contributes to the opening of a gap.

IV. RVB STATE FOR ISOLATED CLUSTERS

In this section, we study the different manifestations of the onset of a RVB-like ground state in the correlation functions. It is known that an RVB state⁴⁹ is formed for small isolated clusters for large values of U .^{47,70} We will start by considering the four-level model, where there are two \mathbf{K} -states on the cluster, $(\pi, 0)$ and $(0, \pi)$, each coupling to one bath state. This model shows the relations between the real space correlations and the correlation function B in a particularly transparent way. We then extend our analysis to larger isolated clusters, where the physics is similar. Eventually, the general connection to the spectral properties of the systems will be discussed in Sec. V.

A. Four-level model

In the limit of very large U and for $\Delta U > 0$, the ground-state of the four-level model takes the form

$$|\Phi\rangle = \frac{1}{2} (c_{1c\uparrow}^\dagger c_{1c\downarrow}^\dagger - c_{2c\uparrow}^\dagger c_{2c\downarrow}^\dagger) (c_{1b\uparrow}^\dagger c_{1b\downarrow}^\dagger - c_{2b\uparrow}^\dagger c_{2b\downarrow}^\dagger) |\text{vac}\rangle, \quad (41)$$

where the indices 1 and 2 refer to orbitals with $\mathbf{K} = (\pi, 0)$ and $(0, \pi)$, respectively. The ground state wave function is a product of a cluster and a bath wave function, and the hopping between the cluster and the bath is unimportant in this limit. In this sense we can talk about a localization

of two electrons on the cluster. Writing explicitly the cluster part of the wave function we get

$$|\Phi_c\rangle = \frac{1}{\sqrt{2}}(c_{(\pi,0)\uparrow}^\dagger c_{(\pi,0)\downarrow}^\dagger - c_{(0,\pi)\uparrow}^\dagger c_{(0,\pi)\downarrow}^\dagger)|\text{vac}\rangle. \quad (42)$$

We also note, that the corresponding state for a four-site cluster with the $\mathbf{K} = (0, 0)$ orbital occupied is given by

$$|\psi_{\text{loc}}\rangle = \frac{1}{\sqrt{2}}(c_{(\pi,0)\uparrow}^\dagger c_{(\pi,0)\downarrow}^\dagger - c_{(0,\pi)\uparrow}^\dagger c_{(0,\pi)\downarrow}^\dagger)c_{(0,0)\uparrow}^\dagger c_{(0,0)\downarrow}^\dagger|\text{vac}\rangle, \quad (43)$$

In Ref. 57 it was shown that this is a good approximation to the calculated state for a four-site cluster for moderate values of U . It was also shown that this state is fairly closely related to a RVB state for the four-site cluster. We therefore refer to the states in Eqs. (42, 43) as RVB-like states, although the RVB state is not yet fully developed for values of U of interest here. This is discussed further in Appendix B. The states have singlet character.

If, for large U , $\Delta U < 0$ instead, the ground-state of the four-level model takes the form

$$|\Phi\rangle = \frac{1}{\sqrt{3}}[c_{1c\uparrow}^\dagger c_{2c\uparrow}^\dagger c_{1b\downarrow}^\dagger c_{2b\downarrow}^\dagger - \frac{1}{2}(c_{1c\uparrow}^\dagger c_{2c\downarrow}^\dagger + c_{1c\downarrow}^\dagger c_{2c\uparrow}^\dagger) \times (c_{1b\uparrow}^\dagger c_{2b\downarrow}^\dagger + c_{1b\downarrow}^\dagger c_{2b\uparrow}^\dagger) + c_{1c\downarrow}^\dagger c_{2c\downarrow}^\dagger c_{1b\uparrow}^\dagger c_{2b\uparrow}^\dagger]|\text{vac}\rangle. \quad (44)$$

Here the c part is degenerate and has triplet character and it couples to the bath in a Kondo-like way. In this case, even in the large U limit we cannot separate the wave function as a product of a cluster and a bath part, and hopping remains essential for the character of the state. We can then not talk about localization in the sense used below Eq. (41).

In order to clarify the connection with the correlations in real space, we first convert the $(\pi, 0)$ and $(0, \pi)$ states to real space, using a four site cluster to represent the levels. Putting sites 1 and 2 in the x -direction and 1 and 4 in the y -direction (see inset in Fig. 1), we have

$$\begin{aligned} \phi_{(\pi,0)} &= \frac{1}{2}(|1\rangle - |2\rangle + |4\rangle - |3\rangle) \\ \phi_{(0,\pi)} &= \frac{1}{2}(|1\rangle + |2\rangle - |4\rangle - |3\rangle) \end{aligned} \quad (45)$$

The wave function in Eq. (42) then takes the (real space) form

$$|E_0(N_{\text{el}})\rangle = \frac{1}{2\sqrt{2}}[-(|1\uparrow 2\downarrow\rangle - |1\downarrow 2\uparrow\rangle) + (|1\uparrow 4\downarrow\rangle - |1\downarrow 4\uparrow\rangle) + (|2\uparrow 3\downarrow\rangle - |2\downarrow 3\uparrow\rangle) - (|3\uparrow 4\downarrow\rangle - |3\downarrow 4\uparrow\rangle)] \quad (46)$$

The two terms within each parenthesis (...) form a valence bond (VB), and the sum over all nearest neighbor VB gives the nearest neighbor RVB form. It is then clear that the operator in Eq. (33) couples the terms *within* each parenthesis very efficiently. The different contributions to $B_{\uparrow\downarrow}$ add up coherently (with a negative sign) for $\mathbf{K} - \mathbf{K}' = (\pi, \pi)$ and combine constructively with

TABLE II: Re $A_{\uparrow\downarrow}(\mathbf{K}, \mathbf{K}', \mathbf{Q})$ for the four-level model in the large U and $T \rightarrow 0$ limits and for $\Delta U > 0$. $\mathbf{K} = (\pi, 0)$. The table also shows Re $B_{\uparrow\downarrow}(\mathbf{K}, \mathbf{K}')$ and Re $C_{\text{sp}}(\mathbf{K}, \mathbf{Q})$.

\mathbf{Q}	$\mathbf{K}' = \mathbf{K} + (\pi, \pi)$	$\mathbf{K}' = \mathbf{K}$	$C_{\text{sp}}(\mathbf{K}, \mathbf{Q})$
(π, π)	-1.0	0.0	-1.5
$(0, 0)$	-0.5	0.5	0.5
$B_{\uparrow\downarrow}(\mathbf{K}, \mathbf{K}')$	-1.5	0.5	

TABLE III: Re $A_{\uparrow\downarrow}(\mathbf{K}, \mathbf{K}', \mathbf{Q})$ for the four-level model in the large U and $T \rightarrow 0$ limits and for $\Delta U < 0$. $\mathbf{K} = (\pi, 0)$. The table also shows Re $B_{\uparrow\downarrow}(\mathbf{K}, \mathbf{K}')$ and Re $C_{\text{sp}}(\mathbf{K}, \mathbf{Q})$.

\mathbf{Q}	$\mathbf{K}' = \mathbf{K} + (\pi, \pi)$	$\mathbf{K}' = \mathbf{K}$	$C_{\text{sp}}(\mathbf{K}, \mathbf{Q})$
(π, π)	0.00	-0.33	-0.5
$(0, 0)$	-0.16	-0.50	-0.5
$B_{\uparrow\downarrow}(\mathbf{K}, \mathbf{K}')$	-0.16	-0.83	

the trivial term $\langle n_{\mathbf{K}'\downarrow} \rangle$, while for $\mathbf{K} - \mathbf{K}' = 0$ there is a destructive interference with term $\langle n_{\mathbf{K}'\downarrow} \rangle$. The result is a large negative contribution for $\mathbf{K} - \mathbf{K}' = (\pi, \pi)$ and a small result for $\mathbf{K} - \mathbf{K}' = 0$. The results for $B_{\uparrow\downarrow}(\mathbf{K}, \mathbf{K}')$ are shown in Table II. The corresponding results for $A_{\uparrow\downarrow}(\mathbf{K}, \mathbf{K}', \mathbf{Q})$ and $C_{\text{sp}}(\mathbf{K}, \mathbf{Q})$ are also reported there: The main contribution to $B_{\uparrow\downarrow}[\mathbf{K}, \mathbf{K} + (\pi, \pi)]$ originates from $A_{\uparrow\downarrow}[\mathbf{K}, \mathbf{K} + (\pi, \pi), (\pi, \pi)]$. The same holds for $C_{\text{sp}}(\mathbf{K}, \mathbf{Q})$ at the corresponding transfer momentum $\mathbf{Q} = (\pi, \pi)$.

The large value of $A_{\uparrow\downarrow}[(\pi, 0); (0, \pi); (\pi, \pi)]$ can also be easily understood in reciprocal space by applying the definition of A in Eq. (20) to the wave function in Eq. (42), because the operator in Eq. (20) directly couples the two terms in Eq. (42).

For $\Delta U < 0$ the behavior is completely different, as seen in Table III. $|B_{\uparrow\downarrow}(\mathbf{K}, \mathbf{K}')|$ is now particularly large for $\mathbf{K}' = \mathbf{K}$, and the main contribution to this B comes from $\mathbf{Q} = (0, 0)$. At the same time, $C_{\text{sp}}(\mathbf{K}, \mathbf{Q})$ is now the same for $\mathbf{Q} = (0, 0)$ and (π, π) . Further, in contrast to almost of all other cases we consider in this work, we note that here $C_{\text{sp}}(\mathbf{K}, \mathbf{Q} = (\pi, \pi))$ differs significantly from $B_{\uparrow\downarrow}(\mathbf{K}, \mathbf{K} + (\pi, \pi))$. This happens because, as we already mentioned in Sec. II, in the four-level model the SU(2) symmetry is violated and, thus, the related equivalence relations between B and C are not guaranteed a priori.⁷¹

TABLE IV: Re $B_{\uparrow\downarrow}(\mathbf{K}, \mathbf{K}')$ at $T = 0$ for an isolated cluster with N_c sites in the large U limit according to Eq. (33).

Model	$\mathbf{K}' = \mathbf{K} + (\pi, \pi)$	$\mathbf{K}' = \mathbf{K}$
Four-level ($N_c = 2$)	-1.5	0.50
$N_c = 4$	-1.09	0.25
$N_c = 8$	-0.88	0.13
$N_c = 16$	-0.51	0.06

B. Isolated $N_c = 4$ cluster

We next consider the $N_c = 4$ case in the large U limit. The wave function of the cluster takes the RVB form, which can be written as

$$\begin{aligned} \psi = & \frac{1}{\sqrt{3}} [c_{\mathbf{R}_1\uparrow}^\dagger c_{\mathbf{R}_2\downarrow}^\dagger c_{\mathbf{R}_3\uparrow}^\dagger c_{\mathbf{R}_4\downarrow}^\dagger + c_{\mathbf{R}_1\downarrow}^\dagger c_{\mathbf{R}_2\uparrow}^\dagger c_{\mathbf{R}_3\downarrow}^\dagger c_{\mathbf{R}_4\uparrow}^\dagger] |\text{vac}\rangle \\ & - \frac{1}{2\sqrt{3}} [c_{\mathbf{R}_1\uparrow}^\dagger c_{\mathbf{R}_2\downarrow}^\dagger c_{\mathbf{R}_3\downarrow}^\dagger c_{\mathbf{R}_4\uparrow}^\dagger + c_{\mathbf{R}_1\downarrow}^\dagger c_{\mathbf{R}_2\uparrow}^\dagger c_{\mathbf{R}_3\uparrow}^\dagger c_{\mathbf{R}_4\downarrow}^\dagger \\ & + c_{\mathbf{R}_1\uparrow}^\dagger c_{\mathbf{R}_2\uparrow}^\dagger c_{\mathbf{R}_3\downarrow}^\dagger c_{\mathbf{R}_4\downarrow}^\dagger + c_{\mathbf{R}_1\downarrow}^\dagger c_{\mathbf{R}_2\downarrow}^\dagger c_{\mathbf{R}_3\uparrow}^\dagger c_{\mathbf{R}_4\uparrow}^\dagger] |\text{vac}\rangle \end{aligned} \quad (47)$$

Here we will focus again on the most relevant case, where $\mathbf{K} = (\pi, 0)$ and $\mathbf{K}' = (\pi, 0)$ or $(0, \pi)$. Applying the operator in Eq. (33), leads to couplings involving NN bonds and connecting terms between the first row and the second or third rows. Using the large U limit [Eq. (28)], we obtain $B_{\uparrow\downarrow}(\mathbf{K}, \mathbf{K}') = -0.92$ for $\mathbf{K}' = \mathbf{K} + (\pi, \pi)$ and $+0.42$ for $\mathbf{K}' = \mathbf{K}$. Although the wave function in Eq. (47) has no second nearest neighbor RVB, couplings are generated between the terms in the second and third rows, in particular second nearest-neighbor couplings. The function $B_{\uparrow\downarrow}[\mathbf{K}, \mathbf{K} + (\pi, \pi)]$ is therefore not a perfect measure of the RVB nature of the ground-state. These terms, however, are rather small (0.17), and the total contributions to $B_{\uparrow\downarrow}[\mathbf{K}, \mathbf{K}']$ change from -0.92 to -1.09 and from $+0.42$ to $+0.25$, respectively (cf. Table IV).

To double-check the reliability of our approximations, we have also calculated results for $A_{\uparrow\downarrow}(\mathbf{K}, \mathbf{K}', \mathbf{Q})$ for a $N_c = 4$ isolated cluster at $T = 0$ for a finite $U = 1.6$ eV and for $U = \infty$ without using any of the assumptions behind Eq. (33). The states of the isolated cluster were calculated using exact diagonalization, and expressed in terms of orbitals with well-defined \mathbf{K} -values. Eq. (26) can then easily be applied directly. Table V compares the results with the approximate formula Eq. (33). The approximate results are generally smaller (in absolute values) than the exact results for $U = 1.6$ eV. This is primarily due to the approximation in Eq. (28) for the eigenvalues, which leads to an underestimate in Table V by a factor 0.6 for $U = 1.6$ eV. Taking this into account, the agreement between the approximate and the exact results is fairly good. For $U = \infty$, Eq. (33) becomes exact, and gives the exact results shown in the table. The table also shows the corresponding numerical results for C_{sp} , demonstrate that this quantity also becomes substantially large (and negative) for $\mathbf{Q} = (\pi, \pi)$, consistent with its equivalence to $B_{\uparrow\downarrow}[\mathbf{K}, \mathbf{K} + (\pi, \pi)]$ in SU(2)-symmetric calculations.

For $N_c = 4$ and $U = 1.6$ eV, the $\mathbf{K} = (0, 0)$ level is approximately doubly occupied, and the remaining two electrons form a wave function similar to the cluster part of Eq. (42) for the four-level model,⁵⁷ as shown in Eq. (43). It is then natural that the results are similar to the ones for the four-level model.⁷² In particular, there is an important contribution to $B_{\uparrow\downarrow}[\mathbf{K}, \mathbf{K} + (\pi, \pi)]$ from $\mathbf{Q} = (\pi, \pi)$. For $U = \infty$ all levels are occupied

TABLE V: $\text{Re } A_{\uparrow\downarrow}(\mathbf{K}, \mathbf{K}', \mathbf{Q})$ for an $N_c = 4$ isolated cluster and $\mathbf{K} = (\pi, 0)$. Exact results [Eq. (26)] and results obtained using the approximate formula in Eqs. (33) are shown for $U = 1.6$ eV. For $U = \infty$, Eq. (33) becomes exact, and therefore only exact results are shown. The parameters are $t = -0.50$ and $\beta = \infty$. The corresponding values of C_{sp} have been computed for the case $U = 1.6$ eV and $\beta = 60 \text{ eV}^{-1}$.

\mathbf{Q}	$\mathbf{K}' = \mathbf{K} + (\pi, \pi)$		$\mathbf{K}' = \mathbf{K}$		$C_{\text{sp}}(\mathbf{Q})$		
	$U = 1.6 \text{ eV}$	$U = \infty$	$U = 1.6 \text{ eV}$	$U = \infty$			
	Ex	Appr.	Ex	Appr.	Ex		
(π, π)	-0.67	-0.45	-0.38	-0.02	-0.01	-0.04	-1.35
$(0, 0)$	-0.35	-0.23	-0.21	0.31	0.20	0.12	0.37
$(\pi, 0)$	-0.17	-0.13	-0.25	0.03	0.03	0.08	0.01
$(0, \pi)$	-0.17	-0.13	-0.25	0.03	0.03	0.08	0.01
$B(\mathbf{K}, \mathbf{K}')_{\uparrow\downarrow}$	-1.36	-0.95	-1.09	0.35	0.25	0.25	

equally, and Eq. (43) is not a good approximation any more. Then the four-site model becomes quite different from the four-level model.

C. Larger isolated clusters

The dependences of our isolated cluster results on the cluster sizes have also been studied systematically, and the corresponding results have been summarized in Table IV. The calculations have been performed using the approximate formula in Eq. (33) for isolated clusters of size N_c in the large U limit. More specifically Eq. (28) has been used for evaluating the energy differences, and the results should therefore be exact in the large U limit. We also recall that for $N_c = 4$ and 8, the exact ground-state is a NN-RVB state, while for $N_c = 16$ also more distant bonds (neglected in our calculations) play a role.

From the results of Table IV, we can verify, once again, how the RVB character of the states is signaled by the large negative value of $B(\mathbf{K}, \mathbf{K}')$ for $\mathbf{K} - \mathbf{K}' = (\pi, \pi)$ and a smaller positive value for $\mathbf{K} = \mathbf{K}'$.

V. RELATION TO SPECTRA

In this section, we eventually discuss one of the central topics of this work: the relation between real space correlations and spectral functions. Our purpose is to illustrate how changes in these correlation functions are reflected in the spectral function, often in a dramatic way. This will make it possible, in turn, to use spectral functions to extract information about correlation functions. In particular, we will focus here on RVB-like correlations.

In Sec. III, we have already established relations between real space correlation functions and the behavior of the self-energy Σ for small ν_n . The behavior of Σ controls, in turn, the behavior of the spectrum. We have

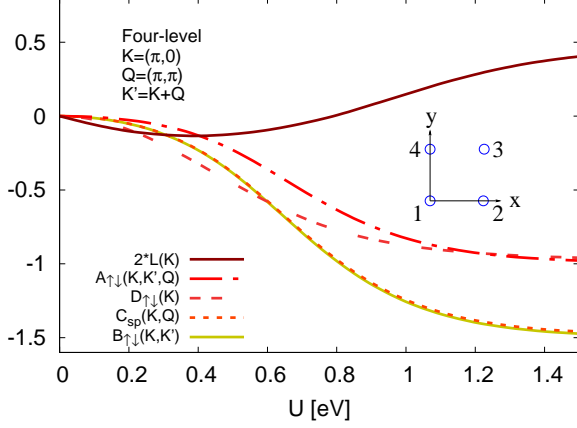


FIG. 1: Real parts of $D_{\uparrow\downarrow}(\mathbf{K})$, $B_{\uparrow\downarrow}(\mathbf{K}, \mathbf{K}')$, $C_{sp}(\mathbf{K}, \mathbf{Q})$ and $A_{\uparrow\downarrow}(\mathbf{K}, \mathbf{K}', \mathbf{Q})$ of the four-level model for $\mathbf{K} = (\pi, 0)$, $\mathbf{K}' = (0, \pi)$ and $\mathbf{Q} = (\pi, \pi)$ as well as $L(\mathbf{K})$. The inset shows the numbering of the sites in Eq. (45). The parameters are $V = -0.1$ eV, $\Delta U > 0$ and $\beta = 60$ eV $^{-1}$.

that

$$\begin{aligned} \text{Im } g(k) &= \text{Im} \frac{1}{i\nu_n - \Delta - \bar{\varepsilon}_{\mathbf{K}} - \Sigma(k)} \\ &= -\nu_n \int \frac{\rho(\mathbf{k}, \varepsilon)}{\varepsilon^2 + \nu_n^2} d\varepsilon, \end{aligned} \quad (48)$$

i.e. $\text{Im } g(k)$ measures the spectral weight over a range ν_n around $\varepsilon = 0$. It is then clear that the presence of large negative value of $\text{Im } \Sigma$ for small ν_n will be reflected in a small or vanishing ρ for small ε , i.e. the system behaves as a non Fermi liquid or, even, as a Mott-Hubbard insulator.

A. Four-level model

We first consider the four-level model for $\Delta U > 0$. Fig. 1 shows various correlation functions for $\mathbf{K} = (\pi, 0)$ (also referred to as level 1c). For small values of U these are all very small. In the case of A , B , C_{sp} and D this is partly because of a prefactor U in Eq. (20), but these quantities remain small even if the prefactor U is divided out. In fact, in the $U \rightarrow 0$ limit the interaction between the two \mathbf{K} -orbitals on the cluster vanishes, and each \mathbf{K} -orbital only interacts with its bath. Therefore these correlation functions would be zero even if the factor U were divided out.

As U is increased, there is also interaction between the cluster \mathbf{K} -orbitals, but the interaction with the bath initially dominates. The increase of U at first leads to a reduction of the double occupancy of each \mathbf{K} , as indicated by $L[(\pi, 0)]$ [Eq. (18)] becoming negative. This

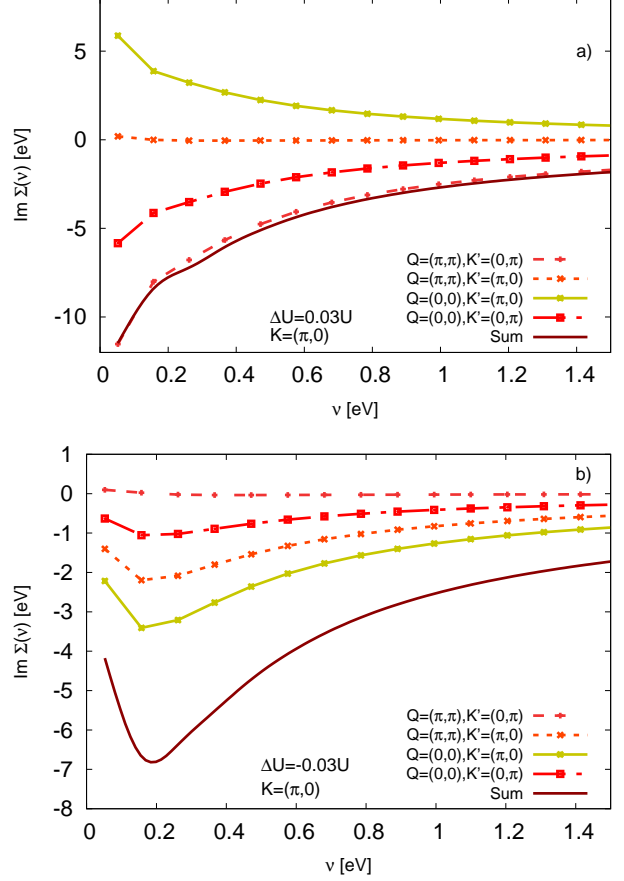


FIG. 2: Contributions to the self-energy of the four-level model for $\mathbf{K} = (\pi, 0)$, labeled according to Eqs. (19, 20) as well as the sum ("Sum") of these contributions for $\Delta U = 0.03$ U (a) and $\Delta U = -0.03$ (b). The figure illustrates the great importance of the sign of ΔU both for the shape of $\Sigma(\nu)$ and for the relative contributions of the different terms Eq. (22). The term for $\mathbf{Q} = (\pi, \pi)$ and $\mathbf{K}' = (0, \pi)$ gives the main contribution to Σ for $\Delta U > 0$, but is almost zero for $\Delta U < 0$. The parameters are $V = -0.1$ eV, $U = 1.6$ eV and $\beta = 60$ eV $^{-1}$.

means that a spin 1/2 state starts to develop in each \mathbf{K} -orbital. This spin is found to have an antiferromagnetic correlation to a spin in its bath.⁴⁷ Thus a Kondo-like state starts to develop for $\mathbf{K} = (\pi, 0)$ and for $\mathbf{K} = (0, \pi)$. The corresponding spectrum has a peak at the Fermi energy.⁴⁷

For intermediate values of $U \sim 1$ eV, $L[(\pi, 0)]$ turns positive, reflecting the fact that the double occupancy of each \mathbf{K} -orbital is now enhanced, instead of being suppressed. The reason is that a state of the type in Eqs. (41, 42) starts to develop, for which each \mathbf{K} -orbital has an enhanced double occupancy. This is an RVB-like state [Eq. (46)], which is strongly correlated. In fact, as U is increased the energy gain from the Kondo effect is reduced and at the same time the energy gain from the formation of the RVB-like state in Eqs. (41, 42) increases, tipping the balance to the RVB-like state.⁴⁷

We proceed now by analyzing the corresponding spectral function, first in the language of Eq. (2), following Ref. 47. For $\Delta U > 0$, if an electron is removed from the cluster in a photoemission process, the RVB-like state is broken up. An electron can then hop in from the bath and form an RVB-like state again. In a similar way, if an electron is added in an inverse photoemission process, an extra electron can hop to the bath, leaving an RVB-like state on the cluster behind. The result is then spectral intensity at the Fermi energy. The crucial question is then what is the probability for forming RVB-like states in the final states after a photoemission or an inverse photoemission process. There are two different paths coupling the ground-state to the final states corresponding to intensity close to the Fermi energy:⁴⁷ (i) For a localized non-degenerate state on the cluster ($\Delta U > 0$), like Eqs. (41, 42), there is destructive interference and a pseudogap at the Fermi energy; (ii) For a localized degenerate state ($\Delta U < 0$), the interference is constructive, leading to a peak at the Fermi energy.^{44–47}

We next discuss the consequences of the formation of the state in Eqs. (41, 42) in terms of the self-energy and the language of Eq. (1). As discussed in Sec. IV A below Eq. (46), the formation of such a state leads to large negative values for the correlation function $A_{\uparrow\downarrow}[\mathbf{K}, \mathbf{K} + (\pi, \pi), (\pi, \pi)]$. This in turn leads to a large negative contribution to $B_{\uparrow\downarrow}[\mathbf{K}, \mathbf{K} + (\pi, \pi)]$, as it would be expected for an RVB-like state according to the discussion in Sec. III C. Finally, this is also responsible for the main contribution to $D_{\uparrow\downarrow}(\mathbf{K})$, which approaches the value -1 for large U . All together, this leads to a large negative value for $\text{Im } \Sigma(\mathbf{K}, \nu_n)$ for small ν_n [Eq. (25)] and, hence, to a small value for the spectral function at the Fermi energy.

Our numerical calculations of the correlation functions A , B and D are reported in Fig. 1, as a function of increasing U , while results for the self-energy Σ of the four-level model are shown in Fig. 2a for a large value of U and $\Delta U > 0$. $\text{Im } \Sigma$ is indeed very negative for small ν_n . The figure illustrates that the main contribution comes from $A_{\uparrow\downarrow}[(\pi, 0), (0, \pi), (\pi, \pi)]$, as could also be seen in Fig. 1. The results in Fig. 2a can be compared with Table II, where $A[(\pi, 0), (0, \pi), (\pi, \pi)]$ dominates. Table II also shows two smaller contributions for $\mathbf{Q} = (0, 0)$ with opposite signs. The corresponding two curves in Fig. 2 also have similar magnitude with opposite signs.

Fig. 2b shows results for $\Delta U < 0$. These results are completely different from the results in Fig. 2a, but agree with Table III. In this case the (absolute) largest contribution comes from $A[(\pi, 0), (\pi, 0), (0, 0)]$. The contribution from $A[(\pi, 0), (0, \pi), (\pi, \pi)]$, which dominates for $\Delta U > 0$, is here very small. In this case, Σ behaves as in a Fermi liquid. This large difference can be traced back⁴⁷ to the degenerate character of the lowest cluster state for $\Delta U < 0$, in contrast to the non-degenerate character for $\Delta U > 0$.

These two (opposite) cases illustrate how the spectrum can depend very sensitively on small modifications in the

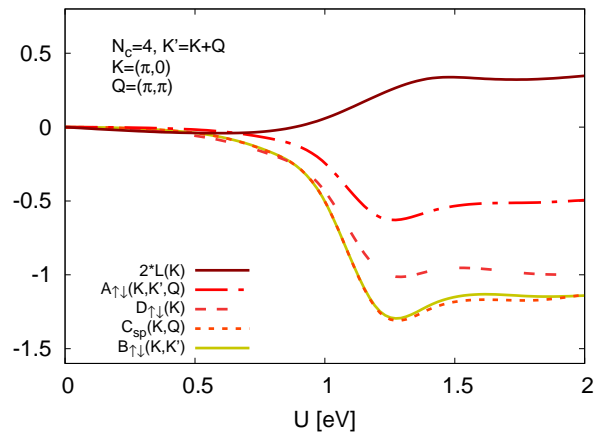


FIG. 3: Real parts of $B_{\uparrow\downarrow}(\mathbf{K}, \mathbf{K}')$, $C_{sp}(\mathbf{K}, \mathbf{Q})$, and $D_{\uparrow\downarrow}(\mathbf{K})$ for $\mathbf{K} = (\pi, 0)$ and for $\mathbf{K}' = (0, \pi)$. The figure also shows $\text{Re } A_{\uparrow\downarrow}(\mathbf{K}, \mathbf{K}', \mathbf{Q})$ for $\mathbf{Q} = (\pi, \pi)$ as well as $L(\mathbf{K})$. The parameters of the corresponding DCA calculation are $N_c = 4$, $t = -0.25$ eV and $\beta = 60$ eV⁻¹. Note that the minor difference between the equivalent values of $B_{\uparrow\downarrow}$ and C_{sp} visible for $U > 1$ is a consequence of the finite numerical precision of the calculation.

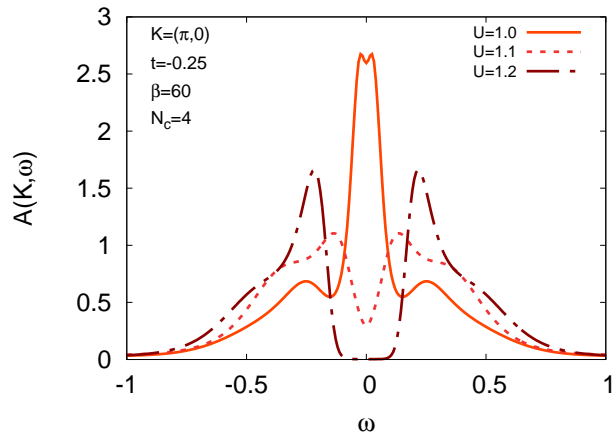


FIG. 4: DCA Spectra for $U = 1.0, 1.1$ and 1.2 eV. The parameters are $N_c = 4$, $t = -0.25$ eV and $\beta = 60$ eV⁻¹.

physical parameters, provided that such modifications lead to a change of ground-state. In Appendix A we give detailed formulas for the spectra.

B. $N_c = 4$

We now turn to the embedded clusters of DCA and study the case $N_c = 4$ first. Fig. 3 shows the quantity $B_{\uparrow\downarrow}[(\pi, 0), (0, \pi)]$, describing the coupling to an RVB-like state, $C_{sp}[(\pi, 0), (\pi, \pi)]$, used in the fluctuation diagnostics, and $D_{\uparrow\downarrow}[(\pi, 0)]$, describing the total contribution to Σ , its largest component $A_{\uparrow\downarrow}[(\pi, 0), (0, \pi), (\pi, \pi)]$ and the correlation function $L[(\pi, 0)]$. These are the same correlation functions as shown in Fig. 1 for the four-level

model. The behavior is very similar. This is not surprising. For large values of U a localized state of the approximate form in Eq. (43) is formed,^{47,57} which is identical to the localized state in Eq. (42) for the four-level model, except for the occupied $\mathbf{K} = (0, 0)$ levels. In fact, by a systematic study⁴⁷ of the correlation functions, it was found that the system also has a similar crossover from a Kondo-like system to a localized system, as for the four-level model.

The largest changes in the correlation functions considered (see Fig. 3) take place between $U = 1.0$ eV and 1.2 eV. Fig. 4 shows the corresponding spectra for $N_c = 4$. For $U = 1.0$ eV there is a peak at the Fermi energy, although there are signs of a pseudogap starting to develop, while for $U = 1.1$ eV there is a pseudogap and for $U = 1.2$ eV a gap. This illustrates that the pseudogap opens up for the values of U where $|B_{\uparrow\downarrow}|$ (and, thus, $|C_{\text{sp}}|$) become large. For $U = 1.2$ eV, $D[(\pi, 0)] \approx -1$, consistent with a very large negative imaginary part of Σ and the opening up of a gap, as discussed below Eq. (25). For large U , the main contribution to $D_{\uparrow\downarrow}[(\pi, 0)]$ comes from $B_{\uparrow\downarrow}[(\pi, 0), (0, \pi)]$, and the contributions from $B_{\uparrow\downarrow}[(\pi, 0), \mathbf{K}']$ for $\mathbf{K}' \neq \mathbf{K} + (\pi, \pi)$ are small. Similarly, if D is expressed as a transfer momentum sum of C_{sp} , the main contribution to $D[(\pi, 0)]$ comes from $C_{\text{sp}}[(\pi, 0), (\pi, \pi)]$ and the contributions from $C_{\text{sp}}[(\pi, 0), \mathbf{Q}]$ for $\mathbf{Q} \neq (\pi, \pi)$ are small.

Just as we could relate the properties of the four-level model to the formation of the localized state in Eq. (42), the crucial common denominator for $N_c = 4$ is the formation of the state in Eq. (43). This leads to a positive value of $L[(\pi, 0)]$ and shows how $|A_{\uparrow\downarrow}[(\pi, 0), (0, \pi), (\pi, \pi)]|$ gets large at the same time as $L[(\pi, 0)]$ goes positive, for reasons already discussed for the four-level model. Thus this specific component of A provides a substantial contribution to $B_{\uparrow\downarrow}[(\pi, 0), (0, \pi)]$, being about half of B . That $|A_{\uparrow\downarrow}[(\pi, 0), (0, \pi), (\pi, \pi)]|$ becomes large when the state Eq. (43) is formed can also be deduced from the definition in Eq. (20). $|A_{\uparrow\downarrow}[(\pi, 0), (0, \pi), (\pi, \pi)]|$ also gives a substantial contribution $C_{\text{sp}}[(\pi, 0), \mathbf{Q}]$. At the same time, that C_{sp} must be also large can be inferred from Eq. (38), relating C_{sp} to antiferromagnetic spin correlations and from the fact that the RVB-like state in Eq. (43) implies, per definition, an appreciable amount of this specific correlation.⁴⁷

On the basis of these considerations, it is clear that the formation of the state in Eq. (43) controls, simultaneously, several correlation functions: (i) L , used in Ref. 47, (ii) C_{sp} , introduced in Ref. 4, as well as (iii) the related quantity B , introduced here to describe more explicitly the coupling to RVB-like real space correlations.

Depending on the different theoretical perspectives, the origin of the pseudogap observed in the DCA spectra of the $2d$ Hubbard model can be ascribed, complementarily, either to antiferromagnetic spin correlations or RVB-like correlations. We must stress here, however, that this is not a contradiction, since the RVB state, as discussed above, does lead to substantial antiferromag-

netic spin correlations, though weaker than in a pure Néel state (for instance, for a cluster with $N_c = 8$ and a large U the difference in strength is about a factor of two.⁴⁸) Thus, in this regime, the two pictures (AF or RVB correlations) simply provide different perspectives on the same physics.

We notice that $A_{\uparrow\downarrow}[\mathbf{K}, \mathbf{K} + (\pi, \pi), (\pi, \pi)]$ gives almost the full contribution to D in the four-level model but only about half the contribution in the $N_c = 4$ model (see Fig. 3), the other 15 combinations of \mathbf{K}' and \mathbf{Q} together contributing the other half. This illustrates the need to switch to summed quantities, such as B and C , for larger values of N_c , as the individual contributions A are reduced with N_c . As discussed in Sec. III these summed quantities can be related to real space correlation functions, and they therefore have a weaker dependence on N_c . The quantity L used in Ref. 47 suffers from similar problems as an individual A , namely of becoming smaller as N_c increases.

C. $N_c = 8$

We now turn to $N_c = 8$. Fig. 5 shows correlation functions for $\mathbf{K} = (\pi, 0)$ and $(\pi/2, \pi/2)$. Similar to the case $N_c = 4$, L first turns negative as U is increased and then positive for larger values of U . As shown in Table I and emphasized in Ref. 47, the coupling to the bath is much weaker for $\mathbf{K} = (\pi, 0)$ and for $(0, \pi)$ than for $(\mp\pi/2, \mp\pi/2)$. Therefore as U is increased, first there is a switch for $\mathbf{K} = (\pi, 0)$ and $(0, \pi)$ from a Kondo-like state to a state where the $(\pi, 0)$ and $(0, \pi)$ orbitals form a state similar to state (43). The loss of the Kondo energy in the $\mathbf{K} = (\pi, 0)$ and $(0, \pi)$ channels is then more than compensated by the substantial energy gain from the correlation of the $\mathbf{K} = (\pi, 0)$ and $(0, \pi)$ cluster orbitals. Over a certain range of U values, the orbitals for $\mathbf{K} = (\pm\pi/2, \pm\pi/2)$, however, still form Kondo-like states with their baths, and they are fairly uncorrelated with other \mathbf{K} -values.⁴⁷ This is also illustrated by $L[(\pi, 0)]$ going from negative to positive values, while $L[(\pi/2, \pi/2)]$ still remains negative over some range of U values. As a result one observes⁴⁷ a pseudogap for $\mathbf{K} = (\pi, 0)$ but not for $\mathbf{K} = (\pm\pi/2, \pm\pi/2)$. For larger values of U also the Kondo states for $\mathbf{K} = (\pm\pi/2, \pm\pi/2)$ are lost and all the cluster orbitals become strongly correlated, forming a localized state. At this point $L[\pi/2, \pi/2]$ also turns positive. Then a spectral gap also opens up for $\mathbf{K} = (\pm\pi/2, \pm\pi/2)$.

Fig. 5 clarifies the progression of the physics with increasing interaction. When $L[(\pi, 0)]$ turns positive, $B_{\uparrow\downarrow}[(\pi, 0), (0, \pi)]$ becomes very negative. This is due to the coupling to a state similar to the state of Eq. (43). The orbitals $(\pm\pi/2, \pm\pi/2)$ are also occupied, but they are more entangled with their baths rather than with the cluster states $(\pi, 0)$ and $(0, \pi)$.⁴⁷ At this point correlation functions involving $(\pi, 0)$ and $(0, \pi)$ take values similar to the ones in the RVB state. For somewhat

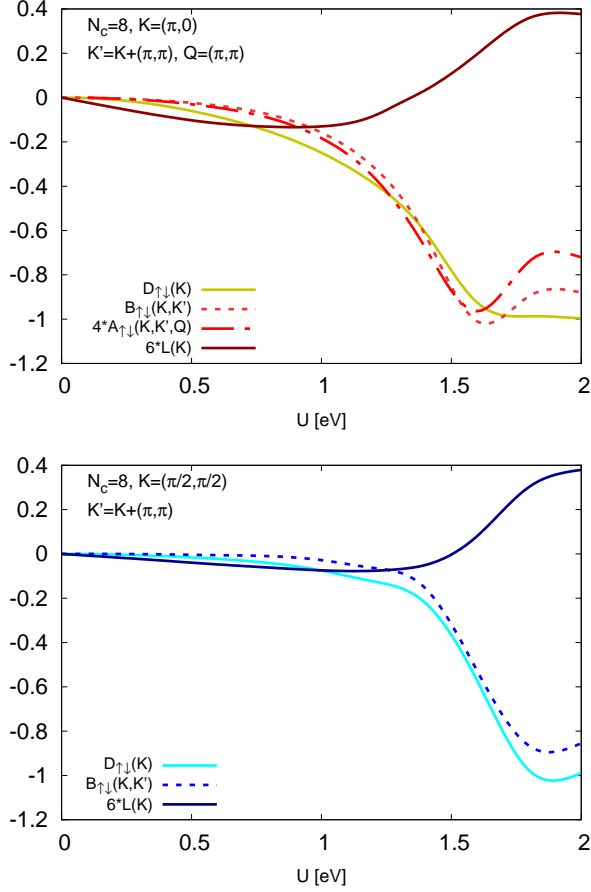


FIG. 5: $\text{Re } B_{\uparrow\downarrow}(\mathbf{K}, \mathbf{K}')$ and $\text{Re } D_{\uparrow\downarrow}(\mathbf{K})$ for $\mathbf{K} = (\pi, 0)$ (upper panel, red, colors online) and $(\pi/2, \pi/2)$ (lower panel, blue colors online) and for $\mathbf{K}' = \mathbf{K} + (\pi, \pi)$. The parameters are $N_c = 8$, $t = -0.25$ eV and $\beta = 60$ eV^{-1} .

larger values of U , $L[(\pm\pi/2, \pm\pi/2)]$ turns positive. Then $B_{\uparrow\downarrow}[(\pi/2, \pi/2), (-\pi/2, -\pi/2)]$ also becomes very negative, and correlation functions involving Fermi surface momenta approximately take on their values for an RVB state. A proper RVB state, however, does not develop until U becomes substantially larger, as discussed in Appendix B.

Fig. 6 shows the spectra for $\mathbf{K} = (\pi, 0)$ and $(\pi/2, \pi/2)$ and for different values of U . In particular, the figure illustrates how a pseudogap appears for $\mathbf{K} = (\pi, 0)$ and $U = 1.6$ eV. In Fig. 5 $|B_{\uparrow\downarrow}[(\pi, 0), (0, \pi)]|$ and $L[(\pi, 0)]$ indeed become large for this value of U , signaling a localization in the $(\pi, 0)$ - $(0, \pi)$ space which causes the pseudogap. For $U = 1.8$ eV, Fig. 6c shows how a spectral gap is opened also for $\mathbf{K} = (\pi/2, \pi/2)$. In Fig. 5 $|B_{\uparrow\downarrow}[(\pi/2, \pi/2), (-\pi/2, -\pi/2)]|$ and $L[(\pi/2, \pi/2)]$ become large for this value of U , signaling that a corresponding localization has also occurred. The evolution of spectra and correlations functions illustrates that the spectra are consistent with the arguments above.

It is important to note, however, that the picture emerging from Fig. 5 is different from the one where the

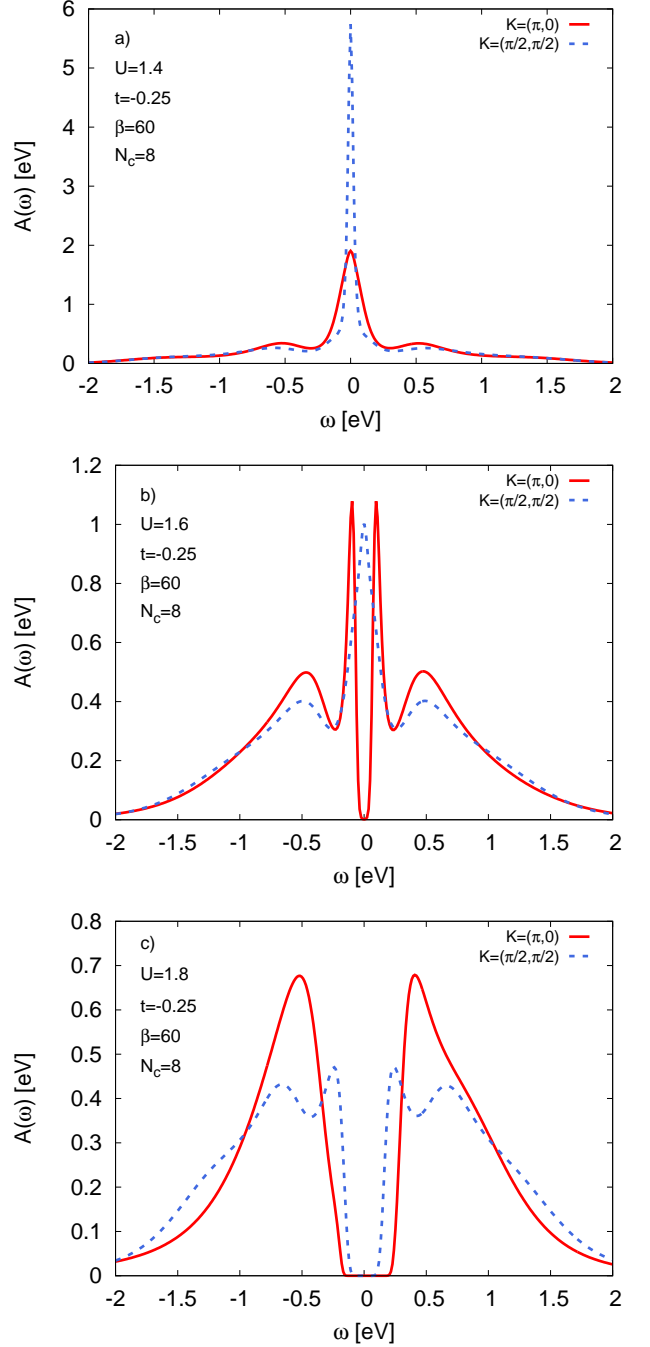


FIG. 6: DCA Spectral functions as a function of \mathbf{K} for $U = 1.4$ (a), 1.6 (b) and $U = 1.7$ (c). The parameters are $N_c = 8$, $t = -0.25$ eV and $\beta = 60$ $(\text{eV})^{-1}$

system is viewed as a set of \mathbf{K} -orbitals coupling to their baths but not to each other. In such a picture there would be a number of independent DMFT calculations for each \mathbf{K} and a series of momentum selective Mott transitions. Correspondingly, one would see how the double occupancy of each \mathbf{K} -state is suppressed as U is increased, and the gap forms because a gap develops also in the bath due to self-consistency. In Fig. 5 the double occu-

pancy in the \mathbf{K} -orbitals is also suppressed ($L(\mathbf{K}) < 0$) for small U , but for larger U the double occupancy is increased ($L(\mathbf{K}) > 0$). This is due to the switch over from Kondo like states to a localized state with strong correlation between $\mathbf{K} = (\pi, 0)$ and $(0, \pi)$, as illustrated by the behavior of L , A and B . This demonstrates that the correlation between different \mathbf{K} -states is crucial for the pseudogap formation. The formation of a pseudogap in the bath happens also here, due to the self-consistency of DCA. However, this is not a general prerequisite for developing a pseudogap in the spectrum of the embedded cluster. In fact, a pseudogap can also form,⁴⁷ if the bath, not calculated self-consistently, is purely metallic, although a somewhat larger U is now required. In this case, the pseudogap forms merely due to the strong correlation between $(\pi, 0)$ and $(0, \pi)$. As U increases, double occupancy of the *sites* is suppressed. This *real* space correlation cannot be described in reciprocal space as a suppression of double occupancy of \mathbf{K} -states, but rather as a correlation between different \mathbf{K} 's. It is then not surprising that this correlation becomes very important for large U .

D. $N_c = 32$

While DCA calculation for larger clusters become numerically more expensive, the additional effort is certainly worth it for the case of a $N_c = 32$. In fact in this DCA cluster, there are *three* inequivalent \mathbf{K} -points on the Fermi surface, $(\pi, 0)$, $(3\pi/4, \pi/4)$ and $(\pi/2, \pi/2)$ (see inset of Fig. 7a), which makes it possible to study in more detail how the pseudogap evolves as U is increased.

Fig. 7 shows the spectra. For $U = 0.9$ eV only $\mathbf{K} = (\pi, 0)$ shows signs of a pseudogap, while there are still metallic peaks at E_F for $\mathbf{K} = (3\pi/4, \pi/4)$ and $(\pi/2, \pi/2)$. Increasing U to 1.0 eV, there is also a pseudogap for $\mathbf{K} = (3\pi/4, \pi/4)$ and, eventually, for $U = 1.1$ eV also $\mathbf{K} = (\pi/2, \pi/2)$ shows an evident non Fermi-liquid behavior.

The observed progression can be understood by studying the couplings [Eq. (10)] to the baths for these three \mathbf{K} points, as shown in Table I. As found before, the coupling for $\mathbf{K} = (\pi, 0)$ is much weaker than for $(\pi/2, \pi/2)$. Table I shows that the point in between, $\mathbf{K} = (3\pi/4, \pi/4)$ indeed has an intermediate coupling. The switch from a Kondo-type of states to a localized state then happens successively for the three \mathbf{K} points as U is increased.

This is illustrated in Fig. 8 showing $D_{\uparrow\downarrow}(\mathbf{K})$, $B_{\uparrow\downarrow}[\mathbf{K}, \mathbf{K} + (\pi, \pi)]$ and $L(\mathbf{K})$. As for smaller N_c , the spectrum for \mathbf{K} obtains a pseudogap shortly after $L(\mathbf{K})$ turns positive. At the same time $B_{\uparrow\downarrow}[\mathbf{K}, \mathbf{K} + (\pi, \pi)]$ and $D_{\uparrow\downarrow}(\mathbf{K})$ become strongly negative.

As U is increased, correlation functions involving $\mathbf{K} = (\pi, 0)$ and $(0, \pi)$ first approach values corresponding to an RVB state. At a somewhat later point this also applies for $\mathbf{K} = (\pm 3\pi/4, \pm \pi/4)$ and $(\pm \pi/4, \pm 3\pi/4)$ and for yet larger values of U for $(\pm \pi/2, \pm \pi/2)$. Thus the gradual development of an RVB state leads the gradual de-

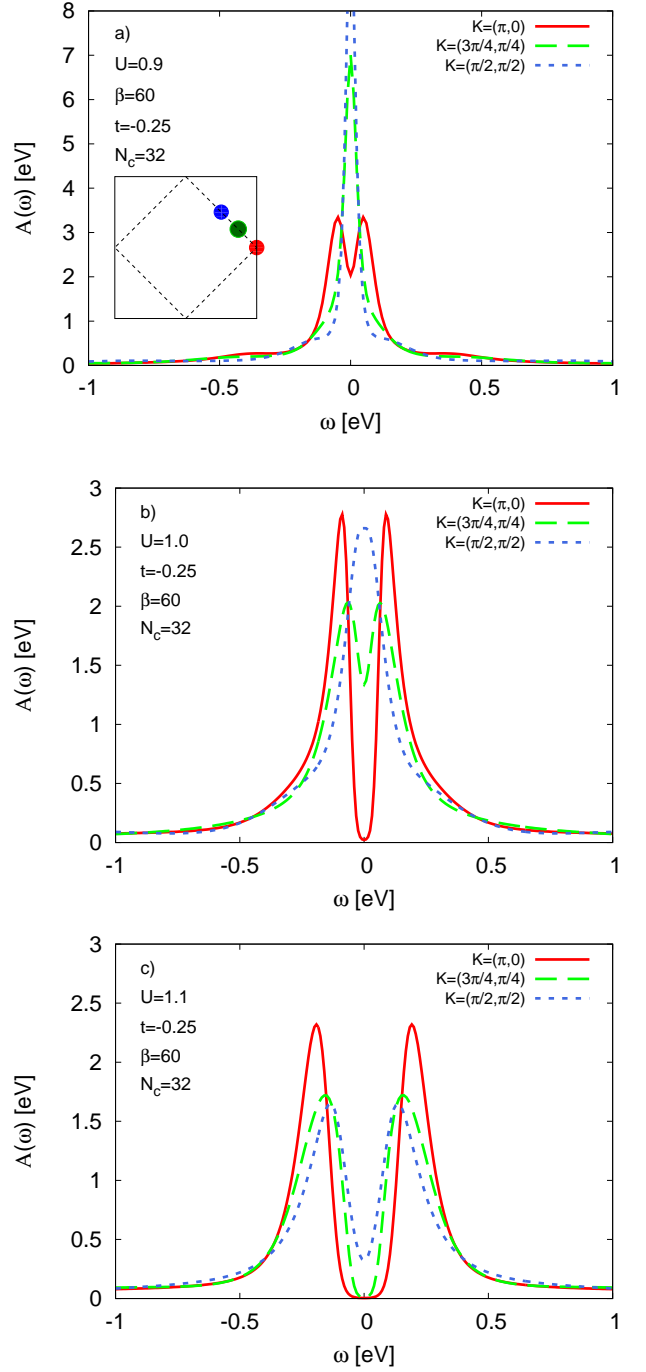


FIG. 7: Spectral functions as a function of \mathbf{K} for $U = 0.9$ eV (a), $U = 1.0$ eV (b) and $U = 1.1$ eV (c). The parameters are $N_c = 32$, $t = -0.25$ eV and $\beta = 60$ (eV)⁻¹.

velopment of a pseudogap for \mathbf{K} -points along the Fermi surface.

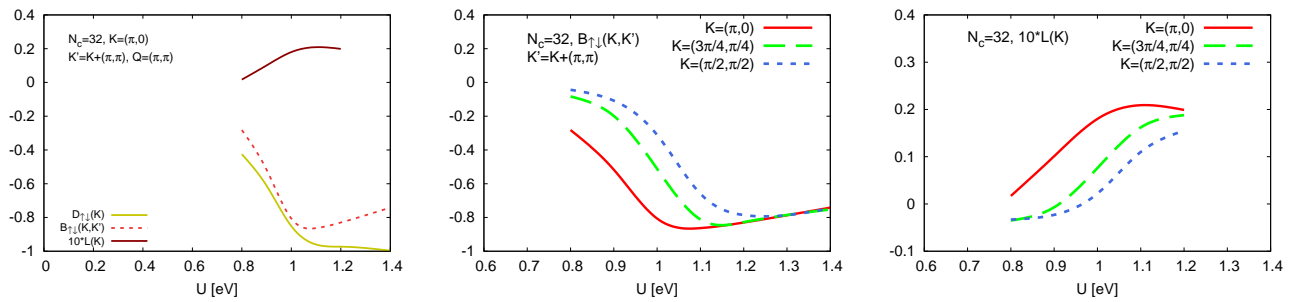


FIG. 8: (colors online) $\text{Re } D(\mathbf{K})$ (left panel), $\text{Re } B(\mathbf{K}, \mathbf{K}')$ (middle panel) and $L(\mathbf{K})$ (right panel) for $\mathbf{K} = (\pi, 0)$ (red solid lines), $\mathbf{K} = (3\pi/4, \pi/4)$ (green long-dashed lines) and $\mathbf{K} = (\pi/2, \pi/2)$ (blue short-dashed lines) and $\mathbf{K}' = \mathbf{K} + (\pi, \pi)$. The parameters of the corresponding DCA calculation are $N_c = 32$, $t = -0.25$ eV and $\beta = 60$ (eV) $^{-1}$.

VI. CONCLUSIONS

In this paper, we have studied the relations between electron spectral functions and real space correlation functions. We used the Schwinger-Dyson equation to establish the connections between the electron self-energy and two-particle vertex functions $F(k, k', q)$, involving summations over k' and q to obtain $\Sigma(k)$. In fact, while F contains a wealth of information about the scattering of the interacting particles, it is a challenging task to disentangle all the effects of these scattering processes on Σ , due to the intrinsic complexity of F . In this work, we have shown that this goal can be achieved through different, but physically equivalent, paths: Either one performs a sum over k' in the equation of motion for Σ , making explicit the contributions as a function of the transferred energy/momentum q (“bosonic fluctuation diagnostics”) or one sums over q and study the contributions to $\Sigma(k)$ as a function of k' (“fermionic fluctuation diagnostics”). While the correlation functions of the two formulations are related by exact expressions, at least for the SU(2)-symmetric case, the latter allows for a more natural interpretation in terms of real space RVB fluctuations.

To improve our physical understanding, we exploited a large U approximation, which allows us to establish more direct, semi-analytical relations between the spectral function and real space correlations. Comparison with numerical calculations for small clusters shows that this approximation is sufficiently accurate for values of U where a spectral gap has developed over the whole Fermi surface in our DCA results for the two-dimensional Hubbard model. In this way, we could relate the spectra to real space charge, spin, superconductivity and RVB correlations. The approach has been applied to the pseudogap regime of the $2d$ Hubbard model, as observed in DCA. It was demonstrated that the development of the pseudogap can be related, in a complementary description, to the formation of strong RVB or of antiferromagnetic correlations, but *not* to superconductivity or charge fluctuations.

In particular, we have performed DCA calculations up

to a 32-site clusters, which has three inequivalent \mathbf{K} -points on the Fermi surface. It is crucial that different \mathbf{K} -orbitals on the cluster have rather different couplings to their baths. Therefore we find that as U is increased, correlation functions first obtain values appropriate for an RVB state for $\mathbf{K} = (\pi, 0)$ and $(0, \pi)$, which have the weakest coupling to their baths. At the same time pseudogaps form for these \mathbf{K} -vectors. The strong interaction between the $(\pi, 0)$ and $(0, \pi)$ for larger values of U is crucial for this result. The same happens for $\mathbf{K} = (\pm 3\pi/4, \pm \pi/4)$ and $(\pm \pi/4, \pm 3\pi/4)$ for a somewhat larger U , due to the stronger coupling to the corresponding baths. Finally this also happens for $\mathbf{K} = (\pm \pi/2, \pm \pi/2)$ for a still larger U , where the coupling to the baths are the strongest.

From a purely algorithmic viewpoint, the systematic derivations presented in this paper demonstrate how it is possible to gain a considerable reduction of the numerical effort for the fluctuation diagnostic calculations (see Eq. (22) and the related discussion).

In summary, we clarify the relation between the evolution of spectra and different correlation functions in the most interesting correlated regime of the $2d$ Hubbard model, where pseudogap features are clearly visible. In doing this, we have made contact to two earlier approaches in Refs. 4 and 47, using the conceptual framework of Eqs. (1) and (2), respectively. From our analysis, it becomes clear how the two approaches indeed capture complementary aspects of the same physics.

VII. ACKNOWLEDGMENTS

We thank M. Capone, P. Chalupa, S. Ciuchi, L. Del Re, J. Le Blanc, and D. Springer for insightful discussions. J.M. acknowledges financial support from (MAT2012-37263-C02-01, MAT2015-66128-R) MINECO/FEDER, EU. AT and TS acknowledge financial support from the Austrian Science Fund (FWF) through the projects SFB-ViCoM F41 (AT) and I 2794-N35 (TS). TS has received funding from the European Research Council under the European Unions Seventh Framework Programme (FP7/2007- 2013) ERC Grant Agreement nr. 319286 (Q-MAC). G.S. acknowledges financial support

by the DFG (SFB 1170 ToCoTronics)

Appendix A: Four-level model. Large U and $\Delta U > 0$

To understand the results for $\Delta U > 0$ in a more transparent way, we consider the large U limit. Then two electrons localize on the cluster, and we can obtain a good description of Σ by considering the isolated cluster. We furthermore assume a small T so that only the lowest state is occupied. For $\Delta U < 0$, the system forms a Kondo-like state with the bath, and even for a large U we cannot simplify the problem by just considering the isolated cluster.

Generally, we can write the Green's function for the cluster level 1 as,

$$[g_{1c1c}(\nu)]^{-1} = [g_{1c1c}^0(\nu)]^{-1} - \Sigma_{1c1c\sigma}(\nu), \quad (\text{A1})$$

where

$$g_{1c1c}^0(\nu) = \frac{1}{i\nu - \varepsilon_c - \frac{V^2}{i\nu - \varepsilon_b + \mu} + \mu} \quad (\text{A2})$$

and

$$\begin{aligned} \Sigma_{1c1c}(\nu) = & -[Zg_{1c1c}(\nu)]^{-1} \sum_{mn} \frac{e^{-\beta E_m} + e^{-\beta E_n}}{i\nu + E_n - E_m} \\ & \times \langle n | [-U_{xx}c_{1c\uparrow}n_{1c\downarrow} - U_{xy}c_{1c\uparrow}n_{2c\downarrow} - Jc_{1c\downarrow}^\dagger c_{2c\downarrow} c_{2c\uparrow} \\ & + Jc_{2c\uparrow}^\dagger c_{2c\uparrow} c_{1c\uparrow} + Jc_{2c\downarrow}^\dagger c_{2c\downarrow} c_{1c\downarrow}] | m \rangle \langle m | c_{1c\uparrow}^\dagger | n \rangle \end{aligned} \quad (\text{A3})$$

We now consider a large U/V and $\Delta U > 0$, so that we can consider the isolated cluster. For a small T we obtain

$$\begin{aligned} \Sigma_{1c1c}(\nu) = & \frac{1}{2g_{1c1c}(\nu)} \left[\frac{U_{xy}}{i\nu - U/2 - 3\Delta U/2 - J/2} \right. \\ & + \frac{U_{xx}}{i\nu + U/2 + 3\Delta U/2 + J/2} \\ & - J \left\{ \frac{1}{i\nu + U/2 + 3\Delta U/2 + J/2} \right. \\ & \left. \left. - \frac{1}{i\nu - U/2 - 3\Delta U/2 - J/2} \right\} \right]. \end{aligned} \quad (\text{A4})$$

Here a term proportional to $U_{xy} - J$ has been neglected. The term

$$J \sum_{\mathbf{k} \neq \mathbf{k}'} c_{\mathbf{k}\uparrow}^\dagger c_{\mathbf{k}\downarrow}^\dagger c_{\mathbf{k}'\downarrow} c_{\mathbf{k}'\uparrow} \quad (\text{A5})$$

in the Hamiltonian couples the two terms in the simplified ground-state [Eq. (42)] particularly efficient. This leads to the large contribution proportional to J in Eq. (A4), which corresponds to $\mathbf{Q} = (\pi, \pi)$ and $\mathbf{K}_1 = (0, \pi)$.

These results can be directly compared with Fig. 2a. For small values of ν the first two terms approximately cancel. These two terms correspond to the processes

$\mathbf{K}_1 = (\pi, 0)$ and $(0, \pi)$ for $\mathbf{Q} = (0, 0)$, which are seen to cancel in Fig. 2a. The term proportional to J corresponds to $\mathbf{Q} = (\pi, \pi)$ and $\mathbf{K}_1 = (0, \pi)$. This term contains two contributions, which approximately add up for small ν . The absolute value of this term is then approximately twice as large as the previous two terms, as is also found in Fig. 2a.

Above we have expressed the self-energy in terms of $\chi_{\uparrow\downarrow}$. We can instead express it in terms of χ_{sp} , as is done in the fluctuation diagnostics.

$$\begin{aligned} \Sigma_{1c1c}(\nu) = & \frac{1}{2g(\nu)} \left[-U_{xx} \frac{1}{i\nu - U/2 - 3\Delta U/2 - J/2} \right. \\ & + J \frac{1}{i\nu - U/2 - 3\Delta U/2 - J/2} \\ & - J \left\{ \frac{1}{i\nu + U/2 + 3\Delta U/2 + J/2} \right. \\ & \left. \left. - \frac{1}{i\nu - U/2 - 3\Delta U/2 - J/2} \right\} \right] \end{aligned} \quad (\text{A6})$$

The first term corresponds to $\mathbf{Q} = (0, 0)$ and $\mathbf{K} = \mathbf{K}' = (\pi, 0)$, the second term to $\mathbf{Q} = (\pi, \pi)$ and $\mathbf{K} = \mathbf{K}' = (\pi, 0)$ and the third term to $\mathbf{Q} = (\pi, \pi)$, $\mathbf{K} = (\pi, 0)$ and $\mathbf{K}' = (0, \pi)$. This is the largest term, showing the importance of $\mathbf{Q} = (\pi, \pi)$ in the fluctuation diagnostics. The first two terms largely cancel each other.

Appendix B: Accuracy of large U approximation

Throughout our work, we have extensively used the large U approximation Eq. (28) in Eqs. (32, 33, 38-40) to obtain a relation between spectra and real space correlation functions for a half-filled system. The accuracy of these approximations is therefore crucial. The approximations were of two types. First we made an approximation for the eigenenergies in Eq. (28) and in the following equations we also assumed that double occupancy can be neglected.

We can now discuss the accuracy of these approximations by comparing general results of the approximations with results in Figs. 1, 3, 5 and 8, which did not use large U approximations. The large U approximations predict that $D_{\uparrow\downarrow} \rightarrow -1$ and that $B_{\uparrow\downarrow}[\mathbf{K}, \mathbf{K} + (\pi, \pi)]$ are independent of \mathbf{K} . We first discuss this for K-points at the Fermi surface. The large U results for B and D then show up in the Figs. 3, 5 and 8 for values of U where the (pseudo)gap has developed. This happens for $U \sim 1.2$ eV ($N_c = 4$), 1.8 eV ($N_c = 8$) and 1.1-1.2 eV ($N_c = 32$), in all cases for $t = -0.25$ eV and $\beta = 60$ eV $^{-1}$. For somewhat smaller values of U , $B_{\uparrow\downarrow}[\mathbf{K}, \mathbf{K} + (\pi, \pi)]$ has an important dependence on \mathbf{K} , also for \mathbf{K} at the Fermi surface. For the \mathbf{K} -points away from the Fermi surface the large- U approximation becomes valid only for substantially larger values of U than above. We have performed calculations for an isolated cluster, since for large U the coupling to the bath plays a small role. For $N_c = 8$ we

find that $B_{\uparrow\downarrow}[\mathbf{K}, \mathbf{K} + (\pi, \pi)]$ becomes independent of \mathbf{K} for all values of \mathbf{K} for $U \simeq 10$ and then $B \simeq -0.7$. We furthermore find that $D_{\uparrow\downarrow} \simeq -1$ for all values of \mathbf{K} for $U \simeq 10$. At this point the RVB state is fully developed.

As U is increased, $B_{\uparrow\downarrow}[\mathbf{K}, \mathbf{K} + (\pi, \pi)]$ first approaches large negative values, as in the RVB state, for \mathbf{K} at

the antinodal point $[(\pi, 0)]$. As U is further increased this gradually happens for \mathbf{K} -vectors moving towards the nodal point. This happens for moderate values of U and it has above been referred to as the formation of an RVB-like state. To fully form an RVB state, however, U has to be increased substantially more.

-
- ¹ L. Hedin and S. Lundqvist, *Effects of Electron-Electron and Electron-Phonon Interactions on the One-Electron States of Solids*, Solid State Physics, **23**, 1, Academic Press, New York (1969)
- ² T. Timusk and B. Statt, Rep. Prog. Phys. **62**, 61 (1999).
- ³ A. Damascelli, Z. Hussain, and Zhi-Xun Shen, Rev. Mod. Phys. **75**, 473 (2003).
- ⁴ O. Gunnarsson, T. Schäfer, J. P. F. LeBlanc, E. Gull, J. Merino, G. Sangiovanni, G. Rohringer, and A. Toschi, Phys. Rev. Lett. **114**, 236402 (2015).
- ⁵ R. Blankenbecker, D. J. Scalapino, and R. L. Sugar, Phys. Rev. D **24**, 2278 (1981).
- ⁶ W. Metzner, M. Salmhofer, C. Honerkamp, V. Meden, and K. Schönhammer, Rev. Mod. Phys. **84**, 299 (2012).
- ⁷ N. E. Bickers, D. J. Scalapino, and S. R. White, Phys. Rev. Lett. **62**, 961 (1989).
- ⁸ V. Janiš, J. Phys.: Condens. Matter **10**, 2915 (1998); Phys. Rev. B **60**, 11345 (1999).
- ⁹ S.X. Yang, H. Fotsó, J. Liu, T. A. Maier, K. Tomko, E. F. D’Azevedo, R. T. Scalettar, T. Pruschke, and M. Jarrell, Phys. Rev. E **80**, 046706 (2009).
- ¹⁰ T. Maier, M. Jarrell, T. Pruschke, and M. H. Hettler, Rev. Mod. Phys. **77**, 1027 (2005).
- ¹¹ W. Metzner and D. Vollhardt, Phys. Rev. Lett. **62**, 324 (1989).
- ¹² A. Georges, G. Kotliar, W. Krauth, and M. Rozenberg, Rev. Mod. Phys. **68**, 13 (1996).
- ¹³ A. I. Lichtenstein and M. I. Katsnelson, Phys. Rev. B **62**, R9283 (2000).
- ¹⁴ G. Kotliar, S.Y. Savrasov, G. Pálsson, and G. Biroli, Phys. Rev. Lett. **87**, 186401 (2001).
- ¹⁵ M. H. Hettler, M. Mukherjee, M. Jarrell, and H. R. Krishnamurthy, Phys. Rev. B **61**, 12739 (2000).
- ¹⁶ A. Toschi, A. A. Katanin, and K. Held, Phys. Rev. B **75**, 045118 (2007).
- ¹⁷ G. Rohringer and A. Toschi, Phys. Rev. B **94**, 125144 (2016).
- ¹⁸ A. N. Rubtsov, M. I. Katsnelson, and A. I. Lichtenstein, Phys. Rev. B **77**, 033101 (2008).
- ¹⁹ H. Hafermann, G. Li, A. N. Rubtsov, M. I. Katsnelson, A. I. Lichtenstein, and H. Monien, Phys. Rev. Lett. **102**, 206401 (2009).
- ²⁰ C. Slezak, M. Jarrell, Th. Maier, and J. Deisz, J. Phys.: Condens. Matter **21**, 435604 (2009).
- ²¹ A. Valli, G. Sangiovanni, O. Gunnarsson, A. Toschi, and K. Held, Phys. Rev. Lett. **104**, 246402 (2010).
- ²² A Valli, T Schäfer, P Thunström, G Rohringer, S Andergassen, G Sangiovanni, K Held, and A Toschi, Phys. Rev. B **91**, 115115 (2015).
- ²³ G. Rohringer, A. Toschi, H. Hafermann, K. Held, V. I. Anisimov, and A. A. Katanin, Phys. Rev. B **88**, 115112 (2013).
- ²⁴ C. Taranto, S. Andergassen, J. Bauer, K. Held, A. Katanin, W. Metzner, G. Rohringer, and A. Toschi, Phys. Rev. Lett. **112**, 196402 (2014); N. Wentzell, C. Taranto, A. Katanin, A. Toschi, and S. Andergassen Phys. Rev. B **91**, 045120 (2015).
- ²⁵ T. Ayrál and O. Parcollet, Phys. Rev. B **92**, 115109 (2015).
- ²⁶ T. Ayrál and O. Parcollet Phys. Rev. B **94**, 075159 (2016).
- ²⁷ T. Timusk and B. Statt, Nature (London) **454**, 1072 (2008).
- ²⁸ K. Haule, A. Rosch, J. Kroha, and P. Wölfle, Phys. Rev. Lett. **89**, 236402 (2002); Phys. Rev. B **68**, 155119 (2003).
- ²⁹ M. Civelli, M. Capone, S. S. Kancharla, O. Parcollet, and G. Kotliar, Phys. Rev. Lett. **95**, 106402 (2005).
- ³⁰ A. Macridin, M. Jarrell, T. Maier, P.R.C. Kent, and E. D’Azevedo, Phys. Rev. Lett. **97**, 036401 (2006).
- ³¹ B. Kyung, S.S. Kancharla, D. Senechal, and A.-M.S. Tremblay, M. Civelli, and G. Kotliar, Phys. Rev. B **73**, 165114 (2006); B. Kyung, and A. M. S. Tremblay, Phys. Rev. Lett. **97**, 046401 (2006).
- ³² S. Sakai, Y. Motome, and M. Imada, Phys. Rev. Lett. **102**, 056404 (2009); S. Sakai, Y. Motome, and M. Imada, Phys. Rev. B **82**, 134505 (2010); S. Sakai, S. Blanc, M. Civelli, Y. Gallais, M. Cazayous, M. A. Masson, J. S. Wen, Z. J. Xu, G. D. Gu, G. Sangiovanni, Y. Motome, K. Held, A. Sacuto, A. Georges, and, M. Imada, Phys. Rev. Lett. **111**, 107001 (2013).
- ³³ M. Ferrero, P.S. Cornaglia, L. De Leo, O. Parcollet, G. Kotliar, and A. Georges, Phys. Rev. B **80**, 064501 (2009).
- ³⁴ P. Werner, E. Gull, O. Parcollet, and A.J. Millis, Phys. Rev. B **80**, 045120 (2009); E. Gull, O. Parcollet, P. Werner, and A.J. Millis, Phys. Rev. B **80**, 245102 (2009); N. Lin, E. Gull, and A.J. Millis, Phys. Rev. B **82**, 045104 (2010); E. Gull, M. Ferrero, O. Parcollet, A. Georges and A. J. Millis, Phys. Rev. B **82**, 155101 (2010).
- ³⁵ A. Liebsch and N.-H. Tong, Phys. Rev. B **80**, 165126 (2009).
- ³⁶ G. Sordi, P. Semon, K. Haule, and A.-M. S. Tremblay, Phys. Rev. Lett. **108**, 216401 (2012).
- ³⁷ V.J. Emery and S.A. Kivelson, Nature **374**, 434 (1995).
- ³⁸ Z. A. Xu, N. P. Ong, Y. Wang, T. Kakeshita, and S. Uchida, Nature **406**, 486 (2000).
- ³⁹ Y. Kosaka, T. Hanaguri, M. Azuma, M. Takano, J. C. Davis, and H. Takagi, Nature Physics **8**, 534 (2012).
- ⁴⁰ Y. Wang, L. Li, M. J. Naughton, G. D. Gu, S. Uchida, and N. P. Ong, Phys. Rev. Lett. **95**, 247002 (2005).
- ⁴¹ M. Civelli, Phys. Rev. Lett. **103**, 136402 (2009); Phys. Rev. B **79**, 195113 (2009).
- ⁴² S. X. Yang, H. Fotsó, S. Q. Su, D. Galanakis, E. Khatami, J. H. She, J. Moreno, J. Zaanen, and M. Jarrell, Phys. Rev. Lett. **106**, 047004 (2011).
- ⁴³ E. Gull, O. Parcollet and A.J. Millis, Phys. Rev. Lett. **110**, 216405 (2013).
- ⁴⁴ M. Ferrero, L. De Leo, P. Lecheminant and M. Fabrizio, J.

- Physics: Cond. Matt. **19**, 433201 (2007).
- ⁴⁵ M. Fabrizio, A. F. Ho, L. De Leo, and G. E. Santoro, Phys. Rev. Lett. **91** 246402 (2003); L. De Leo, M. Fabrizio, Phys. Rev. B **69**, 245114 (2004); PRL **94**, 236401 (2005).
- ⁴⁶ M. Capone, M. Fabrizio, C. Castellani, E. Tosatti, Rev. Mod. Phys. **81**, 943 (2009); M. Capone, M. Fabrizio, C. Castellani, E. Tosatti, Phys. Rev. Lett. **93**, 047001 (2004).
- ⁴⁷ J. Merino and O. Gunnarsson, J. Phys.: Cond. Matter. (Fast Track Commun.) **25**, 052201 (2013); Phys. Rev. B **89**, 245130 (2014)
- ⁴⁸ J. Merino and O. Gunnarsson, arXiv:1310.4597.
- ⁴⁹ S. Liang, B. Doucot, and P. W. Anderson, Phys. Rev. Lett. **61**, 365 (1988).
- ⁵⁰ J. E. Hirsch and R. M. Fye, Phys. Rev. Lett. **56**, 2521 (1986).
- ⁵¹ E. Dagotto, Rev. Mod. Phys. **66**, 763 (1994).
- ⁵² D. J. Scalapino, J. Superconductivity Novel Magnetism, **19**, 195 (2006).
- ⁵³ T. Schäfer, F. Geles, D. Rost, G. Rohringer, E. Arrigoni, K. Held, N. Blümer, M. Aichhorn, and A. Toschi, Phys. Rev. B **91**, 125109 (2015).
- ⁵⁴ E. Koch, G. Sangiovanni, and O. Gunnarsson, Phys. Rev. B **78**, 115102 (2008).
- ⁵⁵ G. Rohringer, A. Valli, and A. Toschi, Phys. Rev. B **86**, 125114 (2012).
- ⁵⁶ W. Wu, M. Ferrero, A. Georges, and E. Kozik, Phys. Rev. B **96**, 041105(R) (2017).
- ⁵⁷ O. Gunnarsson, T. Schäfer, J. P. F. LeBlanc, E. Gull, J. Merino, G. Sangiovanni, G. Rohringer, and A. Toschi, Phys. Rev. B **93**, 245102 (2016).
- ⁵⁸ For a review, see, e.g., N. E. Bickers, Int. J. Mod. Phys. B **5**, 253 (1991) and in *Theoretical Methods for Strongly Correlated Electrons*, edited by D. Senechal, A. Tremblay, and C. Bourbonnais (Springer-Verlag, New York, 2004), chapter 6.
- ⁵⁹ T. Schäfer, G. Rohringer, O. Gunnarsson, S. Ciuchi, G. Sangiovanni, and A. Toschi, Phys. Rev. Lett. **110**, 246405 (2013).
- ⁶⁰ V. Janiš and V. Pokorný, Phys. Rev. B **90**, 045143 (2014).
- ⁶¹ E. Kozik, M. Ferrero, and A. Georges, Phys. Rev. Lett. **114**, 156402 (2015).
- ⁶² A. Stan, P. Romaniello, S. Rigamonti, L. Reining and J.A. Berger New J. of Physics **17** 093045 (2015).
- ⁶³ T. Ribic, G. Rohringer, and K. Held, Phys. Rev. B **93**, 195105 (2016).
- ⁶⁴ T. Schäfer, S. Ciuchi, M. Wallerberger, P. Thunström, O. Gunnarsson, G. Sangiovanni, G. Rohringer, and A. Toschi, Phys. Rev. B **94**, 235108 (2016).
- ⁶⁵ W. Tarantino, P. Romaniello, J. A. Berger, and L. Reining, Phys. Rev. B **96**, 045124 (2017).
- ⁶⁶ O. Gunnarsson, G. Rohringer, T. Schäfer, G. Sangiovanni, and A. Toschi, Phys. Rev. Lett. **119**, 056402 (2017).
- ⁶⁷ J. Vucicevic, N. Wentzell, M. Ferrero, and O. Parcollet, arXiv:1709.10490.
- ⁶⁸ P. Chalupa, P. Gunacker, T. Schäfer, K. Held, and A. Toschi, in preparation.
- ⁶⁹ In the SU(2) symmetric case the correlation functions $B_{\uparrow\downarrow}(\mathbf{k}, \mathbf{K}')$ and $C_{\text{sp}}(\mathbf{K}, \mathbf{Q})$ are directly related, which can be easily seen in the following way: Considering the definition of $C_{\text{sp}}(\mathbf{K}, \mathbf{Q})$ in Eqs. (22) and (36) as well as the SU(2) symmetry represented by the relation⁵⁵ $A_{\uparrow\downarrow}(\mathbf{K}, \mathbf{K}', \mathbf{Q}) = A_{\uparrow\uparrow}(\mathbf{K}, \mathbf{K}', \mathbf{Q}) + A_{\uparrow\downarrow}(\mathbf{K}, \mathbf{K} + \mathbf{Q}, \mathbf{K}' - \mathbf{K})$ we immediately obtain that $C_{\text{sp}}(\mathbf{K}, \mathbf{Q}) = B_{\uparrow\downarrow}(\mathbf{K}, \mathbf{K} + \mathbf{Q})$. From a physical perspective, C_{sp} describes *longitudinal* and $B_{\uparrow\downarrow}$ *transverse* spin fluctuations which are of course the same in a SU(2) symmetric situation.
- ⁷⁰ S. Tang and H.Q. Lin, Phys. Rev. B **38**, 6863 (1988).
- ⁷¹ It is interesting to note that in the previous case ($\Delta U > 0$) the mentioned equivalence between B and C appears to be well preserved (cf. the corresponding values in Table II), although the corresponding four-level model is *not* SU(2)-symmetric. This depends, most likely, on the fact that, for $\Delta U > 0$, the (singlet) nature of the ground state of the model does not change w.r.t. the SU(2)-symmetric case ($\Delta U = 0$), differently from what happens in the case $\Delta U < 0$.
- ⁷² Note, however, that by further increasing U , i.e., for $U \rightarrow \infty$, all levels will be occupied equally, and Eq. (43) is not a good approximation any more. Then the four-site model becomes quite different from the four-level model.